https://doi.org/10.5194/se-2019-162
Preprint. Discussion started: 30 October 2019

Solid Earth Discussions

Cenozoic deformation in the Tauern Window (Eastern Alps, Austria) constrained by in-situ Th-Pb dating of fissure monazite

Emmanuelle Ricchi[1], Christian A. Bergemann[1, 2], Edwin Gnos[2], Alfons Berger[3], Daniela Rubatto[3, 4], Martin J. Whitehouse[5], Franz Walter[6]

[1]*Department of Earth Sciences, University of Geneva, Rue des Maraîchers 13, 1205 Geneva, Switzerland*
[2]*Natural History Museum of Geneva, Route de Malagnou 1, 1208 Geneva, Switzerland*
[3]*Institute of Geological Sciences, University of Bern, Baltzerstrasse 1+3, 3012 Bern, Switzerland*
[4]*Institute of Earth Sciences, University of Lausanne, Geopolis, Lausanne, 1015 Switzerland*
[5]*Swedish Museum of Natural History, Box 50007, SE104-05 Stockholm, Sweden*
[6]*Institut für Erdwissenschaften, Karl-Franzens-Universität, Universitätsplatz 2, 8010 Graz, Austria*

Highlights:

- In-situ dating of hydrothermal monazite-(Ce)
- New constraints on the exhumation of the Tauern metamorphic dome
- Distinct tectonic pulses recorded from East to West

Keywords: Hydrothermal monazite; Alpine fissures; Th-Pb dating; Tauern Window; Protracted deformation

Abstract. Thorium-Pb crystallization ages of hydrothermal monazites from the western, central and eastern Tauern Window provide new insights into Cenozoic tectonic evolution of the Tauern metamorphic dome. Growth domain crystallization ages range from 22.3 ± 0.6 Ma to 7.7 ± 0.9

https://doi.org/10.5194/se-2019-162
Preprint. Discussion started: 30 October 2019

Ma. Three major periods of monazite growth are recorded between ~22 – 19 (peak at 21 Ma), 19 – 15 (major peak at 17 Ma) and 13 – 8 Ma (major peaks at 12, 10 and 8 Ma), respectively interpreted to be related to prevailing N-S shortening, in association with E-W extension, beginning strike-slip movements, and reactivation of strike-slip faulting. Fissure monazite ages largely overlap with zircon and apatite fission tracks data. Besides tracking the thermal evolution of the Tauern dome, monazite dates reflect episodic tectonic movement along major shear zones that took place during the formation of the dome. Geochronological and structural data from the Pfitschtal area in the western Tauern Window show the existence of two cleft generations separated in time by 4 Ma and related to strike-slip to oblique-slip faulting. Moreover, these two phases overprint earlier phases of fissure formation.

1 Introduction

In-situ Th-Pb dating of hydrothermal fissure monazite-(Ce) (in the following simply monazite) has recently been demonstrated to be a reliable method for dating tectonic activity under retrograde metamorphic conditions (Bergemann et al., 2017, 2018, 2019b, 2019a; Berger et al., 2013; Fitz-Diaz et al., 2019; Gasquet et al., 2010; Gnos et al., 2015; Grand'Homme et al., 2016a; Janots et al., 2012; Ricchi et al., 2019). These studies conducted through the entire Alpine orogenic belt allowed constraining tectonic activity in relation with exhumation and fault activity under retrograde lower greenschist to sub-greenschist facies metamorphic conditions.

Hydrothermal fissure monazite, concentrating LREE, Th and U, generally crystallizes in Ca-poor lithologies, outside the stability field of titanite or epidote/allanite. However, once formed, hydrothermal processes may cause dissolution-reprecipitation events leading to resetting of the monazite Th-Pb decay system in parts of the crystal. Chemically and isotopically homogeneous

https://doi.org/10.5194/se-2019-162
Preprint. Discussion started: 30 October 2019

crystals indicate a single, rapid growth episode (e.g., Grand'Homme et al., 2016a). Though crystals showing different growth domains indicative of successive growth episodes are more common. In other cases, parts or entire grains display a patchy zoning due to dissolution-reprecipitation processes (e.g., Ayers et al., 1999; Grand'Homme et al., 2016b). These processes involve element fractionation resulting in crystal zones with often distinct Th/U values (Seydoux-Guillaume et al., 2012).

The advantage of using hydrothermal monazite for dating tectonic activity is related to the high closure temperature of monazite of >800°C, implying that diffusion in monazite is negligible (Cherniak et al., 2004; Gardés et al., 2006, 2007) under P-T conditions at or below 450–500 °C and 0.3 – 0.4 GPa (e.g., Mullis et al., 1994; Mullis, 1996; Sharp et al., 2005) where hydrothermal fissures forms. Recent studies have shown that fissure monazite typically forms between 400-200°C (Gnos et al., 2015; Janots et al., 2019). For this reason, fissure monazite always dates (re)crystallization. Monazite geochronology can thus be utilized to constrain shear and damage zone activity under greenschist and very-low grade metamorphic conditions at least down to 200°C (e.g. Bergemann et al., 2017, 2018; Gnos et al., 2015).

Mineral veins, fissures and clefts (see distinction below) are generally oriented roughly perpendicular to foliation and lineation of their host rocks and may experience prolonged phases of deformation. The fissures either became enlarged by subsequent tectonic activity to form fluid-filled dm- to m- sized clefts, or became completely filled to form mineral veins. Interaction of the fluid that fill the fissures with the surrounding rock leads to dissolution of minerals in the wall rock and mineral precipitation in the fissure. As long as deformation continues, fluid-filled clefts will react to deformation via dissolution-precipitation cycles due to disequilibrium between fluid, rock wall and mineral assemblage within the cleft (e.g. Putnis, 2009). Thus, hydrothermal minerals like monazite do not only grow following the initial fissure formation but form,

https://doi.org/10.5194/se-2019-162
Preprint. Discussion started: 30 October 2019

69 continue to grow, or dissolve during subsequent deformation stages. The timing of these growth
70 or alteration stages may not always be resolvable with the precision of currently available
71 geochronological methods, but different growth stages may be distinguishable through
72 differences in the chemical composition (Grand'Homme et al., 2018). In contrast to the
73 surrounding country rock, the fissures and clefts remain highly reactive at low temperature due to
74 the presence of fluids. For this reasons, deformation steps during brittle deformation may be
75 registered through mineral growth or recrystallization in clefts (e.g., Berger et al., 2013) down to
76 conditions where clay minerals form in fault gauges.
77 The Tauern window (TW) is a thermal and structural dome of the eastern Alps (Fig. 1) exhumed
78 over a period of about 30 Ma starting from the Early Oligocene (e.g. Rosenberg et al., 2018;
79 Schmid et al., 2013). Previous monazite crystallization ages obtained in the eastern subdome of
80 the TW record tectonic activity between 19.0 ± 0.5 and 15.0 ± 0.5 Ma (Gnos et al., 2015). In the
81 current study, monazite geochronology is extended to the entire TW, in order to investigate its
82 Cenozoic deformation history. We particularly aim to establish a chronological record for the
83 younger exhumation history recorded by fissure monazite crystallization, to be compared with
84 known deformation phases.

85 A total of 23 monazite grains together with provenance data, and in some cases host-rock
86 information were dated (Table 1). Seven grains come from the western limb of the TW (INNB1
87 ZEI1, SCHR1, MAYR4, PFIT1, BURG2 and PLAN1; samples 1 to 7; Fig. 1), another seven
88 grains come from the eastern border of the western sub-dome (central TW; SCHEI1, HOPF2,
89 GART1, NOWA3, GART3, STEI2 and KNOR1; samples 8 to 14; Fig. 1) and nine grains were
90 collected in the eastern sub-dome (KAIS6, SALZ18, LOHN4, ORT1, EUKL2, HOAR1,
91 MOKR1, SAND1 and REIS1; samples 15 to 25; Fig. 1, Table 1). In order to capture at best the
92 tectonic activity during the exhumation of the Tauern metamorphic dome, the investigated

https://doi.org/10.5194/se-2019-162
Preprint. Discussion started: 30 October 2019

93 samples were selected in a way that gives priority to sample localities in regions affected by
94 major fault zones and at lithological boundaries. In the following we will discuss the ages in term
95 of sample ID numbers (1-26) provided by Table 1.

96

97 **2 Geologic settings**

98 The Tauern metamorphic and structural dome is the largest tectonic window in the Austroalpine
99 nappe stack, revealing the tectonically underlying Penninic and Subpenninic nappes (e.g. Schmid
100 et al., 2013; Fig. 1). It consists of two sub-domes, with E-W striking upright folds in the internal
101 parts and bordered by two major normal faults, the Katschberg Normal Fault (KNF) in the East
102 and the Brenner Normal Fault (BNF) in the West (Fig. 1). The western sub-dome is dissected by
103 numerous sinistral shear zones (Ahorn Shear Zone (ASZ), Olperer Shear Zone (OSZ), Tuxer
104 Shear Zones (TSZ), Greiner Shear Zone (GSZ) and Ahmtal Shear Zone (AhSZ)) and is bordered
105 by the Salzach-Ennstal-Mariazell-Puchberg fault (SEMP) in the north. The eastern sub-dome is
106 bordered by the sinistral Katschberg Shear Zone System (KSZS) and the Katschberg Normal
107 Fault (KNF) at its northern and eastern margins, by the Mölltal Fault (MöF) at its southern
108 boundary, and cut by the Möll Valley Fault (MVF). The deformation history of these fault
109 complexes will be discussed later.

110 The Tauern evolution started in the Early Paleocene with the accretion and subduction of the
111 Piemont-Liguria Ocean (Matrei Zone; Fig. 1) under the Apulian margin (Austroalpine nappe
112 stack; e.g. Schmid et al., 2004, 2013; D1 deformation of Schmid et al., 2013; Fig.1, Table 2). In
113 the Middle Eocene, the Valais Ocean and parts of the distal European margin (Glockner Nappe
114 System, Eclogite Zone and parts of the Modereck Nappe System; Fig. 1) were equally subducted
115 below the Austroalpine nappe stack and the Matrei Zone accreted during D1 deformation (D2

https://doi.org/10.5194/se-2019-162
Preprint. Discussion started: 30 October 2019

116 deformation of Schmid et al. 2013; Table 2). In the Late Eocene, the D2 thrust formed between
117 the subducted Glockner Nappe System and Modereck Nappe System suffered major folding,
118 resulting in high-pressure units exhumation (D3 deformation of Schmid et al. 2013; Table 2). In
119 the Early Oligocene, this exhumation episode was linked to break-off of the subducting European
120 slab. This was followed by an inversion of slab dynamics at ~23 to 21 Ma (e.g., Rosenberg et al.,
121 2018; Scharf et al., 2013; Schmid et al., 2013; Table 2). The following exhumation of the TW
122 started in the Early to Middle Miocene by Alpine N-S collisional shortening and E-W orogen-
123 parallel extension leading to folding, erosion and lateral extrusion through shear zone
124 development (e.g. Luth and Willingshofer, 2008; Rosenberg and Berger, 2009; Rosenberg and
125 Garcia, 2011; Schmid et al., 2004, 2013; Selverstone, 1988; D5 deformation of Schmid et al.,
126 2013). Previous shear zone age dating in the TW was achieved using different geochronometers:
127 phengite isochron corrected Rb-Sr dating (20 Ma; Blanckenburg et al., 1989), isochron corrected
128 Rb-Sr dating on white mica (39 – 16 Ma; Glodny et al., 2008), Sm–Nd dating on garnet (27.5 –
129 20 Ma; Pollington and Baxter, 2010, 2011) and $^{40}Ar/^{39}Ar$ dating on mica (35 – 28 Ma; Urbanek et
130 al., 2002). A recent detailed study by Schneider et al. (2013) using texturally-controlled in-situ
131 $^{40}Ar/^{39}Ar$ dating of syn-kinematic phengite and K-feldspar returned ages between 33 – 15, 24 –
132 12 and 20 – 7 Ma recording deformation along three major shear zones (ASZ, TSZ and GSZ
133 respectively) of the western sub-dome.

134 **Sample location**

135 Fissure monazite is rare and difficult to find, meaning that this study could not have been
136 conducted without the help of crystal searchers who provided samples. Fissure monazites were
137 selected to cover all parts of the TW areas with known shear zones within it. It was, however,
138 unfortunately not possible to obtain exact coordinates for all of the samples (Table 1). This is due

https://doi.org/10.5194/se-2019-162
Preprint. Discussion started: 30 October 2019

to the rarity of fissure monazite, so that some samples were obtained from old finds or collections. In other cases, the crystal searcher could not anymore precisely identify the fissure in which the monazite was found. These samples are marked with "approx." in Table 1. We could therefore only revisit some of the sample locations in order to add structural information. Experience from other parts of the Alps (e.g. Bergemann et al., 2017, 2019; Ricchi et al., 2019) shows that fissure monazite sampled within the damage or central zones of a shear zone generally records shear zone activity well. Information on the source localities, host-rocks, degree of alpine metamorphism and mineral associations is in Table 1.

3 Methods

The crystals where polished individually on a lapidary disk and embedded in epoxy together with the monazite standard "44069" (425 Ma, Aleinikoff et al., 2006), following the same procedure as Bergemann et al. (2017). Backscatter electron (BSE) images were acquired in order to investigate the internal textural features of each grain (e.g. zoning, evidences of alteration, etc.) using an EDS-equipped JEOL JSM7001F and a Zeiss DSM940A electron microscope at the University of Geneva with a beam current of 3.5 nA and acceleration voltage of 15kV. BSE images helped in the selection of Secondary-Ion Mass Spectrometry (SIMS) spot analysis points, carefully placed in distinct growth domains.

Ion probe U-Th-Pb analyses of 15 monazite crystals were conducted at the SwissSIMS Ion microprobe facility, University of Lausanne, Switzerland (Tables 1 and 3) and analyses of another 8 crystals were performed at the Nordsim facility, Swedish Museum of Natural History, Stockholm (Tables 1 and 4). Both laboratories are equipped with a Cameca IMS 1280-HR instrument. The instruments were run following the procedure of Janots et al. (2012), applying a -

https://doi.org/10.5194/se-2019-162
Preprint. Discussion started: 30 October 2019

13 kV O^{2-} primary beam, an intensity of ca. 3 and 6 nA focused on the sample (SwissSIMS and Nordsim, respectively) to produce a spot of 15-20 micron in diameter. A mass resolution of 4300–5000 (M/ΔM, at 10% peak height) and an energy window 40 eV were applied, with data collection in peak hopping mode using an ion-counting electron multiplier. The data were standardised to 44069 monazite and the uncertainty on the standard $^{208}Pb/^{232}Th$ – ThO/Th calibration in each session was 1.0 to 1.8 %.

A ^{207}Pb and ^{204}Pb common lead (Pbc) correction calculated at time zero was applied to the data acquired at the SwissSIMS (Table 3) and Nordsim (Table 4) respectively, as described in Ricchi et al. (2019), using the terrestrial Pb evolution model of Stacey and Kramers (1975). The SQUID (Ludwig, 2009) and Cameca Customisable Ion Probe Software (CIPS) were respectively used for data reduction. Calculation of weighted mean ages (based on ^{207}Pb and ^{204}Pb Pbc correction for the data acquired at the SwissSIMS and Nordsim respectively) and plotting was carried out using the program IsoPlot Ex 4.1 (Ludwig, 2003). Single and weighted mean ages (or average ages) are quoted at the 1 sigma and at 95% confidence level in the text, respectively.

Weighted mean ages were calculated for each growth domain following the approach of Bergemann et al. (2019b, 2019a, 2018, 2017) and Ricchi et al. (2019). Distinct chemical and textural domains were carefully defined in each grain based on Th as function of U plots and BSE images information. Since fissure monazite is dissolved and re-precipitated under changing chemical conditions (e.g. Grand'Homme et al., 2018), spot analyses affected by Pbc (resulting in older dates directly related to higher Pbc), inclusions or with high uncertainty were removed from the dataset and marked in italic in Tables 3 and 4. However, spot dates located on dissolution trails, generally providing younger dates, were considered in the age ranges because they likely record a later phase of monazite crystallization.

https://doi.org/10.5194/se-2019-162
Preprint. Discussion started: 30 October 2019


Solid Earth Discussions

185

186 **4 Results**

187 Fissures and clefts develop close to the brittle-ductile transition (< 450°C, Mullis, 1996) and are
188 usually oriented perpendicular to the foliation and lineation of the host-rock (Gnos et al., 2015).
189 Fissures are generally straight when they form and commonly develop a more open shape (clefts)
190 with rounded surfaces (e.g. Ricchi et al., 2019) when the stress field retains the same orientation.
191 However, they may show complex shape when the stress field direction changes during
192 deformation. Fluid inclusion study (e.g. , Mullis, 1996) show that clefts generally suffered several
193 deformation episodes.

194

195 **4.1 Field observations**

196 An example of deformed fissures and different stages of fissure formation is well exposed in
197 outcrops along the road leading to Pfitscherjoch (in vicinity to the PFIT1 sample locality, Western
198 TW; Table 1), where two fissure generations are present (Fig. 2a and b). In this outcrop an earlier
199 fissure generation (C_2, green ellipses) is partly deformed during subsequent deformation, and a
200 younger generation of fissures (C_3, blue ellipses) that formed in a differently-oriented stress field
201 is also present. Sub-horizontal fissures (C_3) are linked to a strongly inclined lineation (L_3, blue
202 arrows), whereas older sub-vertical fissures (C_2) are related to strike-slip lineation (L_2, green
203 arrows). The older fissures are wider, and sigmoidal in shape and contain muscovite, which is not
204 found in the younger fissures. In some cases younger fissures crosscut older ones (Fig. 2b).
205 Moreover, the orientation of the foliation ($S_{2,3}$, Fig. 2c) of these two fissure generations (C_2 and
206 C_3) is different from the foliation (S_1, Fig. 2c) of early fissure formation mainly observed in the

https://doi.org/10.5194/se-2019-162
Preprint. Discussion started: 30 October 2019

207 eastern part of the TW (C_1, Fig. 2c, discussed below). This suggests that in the Pfitscherjoch area,
208 early fissures C_1 were overprinted by younger tectonic movements.

209 The large majority of the fissures present in all the investigated localities are oriented sub-
210 vertically (C_1 and C_2 type on figure 3c), roughly striking NE-SW. This would indicate a similar
211 stress orientation for the development of this fissure type, which is in line with paleostress
212 orientations provided by Bertrand et al. (2015). However, even if all sub-vertical fissures are sub-
213 parallel, at least two generations exist. (i) Early sub-vertical fissures (C_1, Fig. 2c) are related to
214 flat foliation (S_1) and E-W stretching lineation (L_1), these are oriented perpendicular to the main
215 fold axis (and lineation) of the TW and are associated with E-W extension (e.g. Gnos et al., 2015;
216 Rosenberg et al., 2018; Schneider et al., 2013). (ii) Younger sub-vertical fissures (C_2, Fig. 2c) are
217 associated with sub-vertical E-W oriented foliation (S_2) and flat to inclined lineation (L_2), and are
218 oriented perpendicular to strike-slip faults (mainly in the western part of the TW; Fig. 2c. (iii) A
219 third generation of fissures (C_3, Fig. 2c) is observed, for example, in the Pfitscherjoch locality
220 (Fig. 2a and b) and is perpendicular to the sub-vertical C_1 and C_2 fissures. This third and sub-
221 horizontal fissure orientation observed in the Pfitscherjoch locality displays subvertical E-W
222 oriented foliation (S_3) and down-dip lineation (L_3). Stretching lineation related to the BNF
223 activity is sub-parallel to C_3 lineation, however its foliation is oriented N-S (Fig. 2c). We suggest
224 that sub-horizontal C_3 fissures are related to oblique-slip movements in line with the observed E-
225 W oriented foliation and not to the BNF activity.

226

227 **4.2 Monazite dating and composition**

228 The monazite grains selected for in-situ Th-Pb dating are mm-sized and, when BSE zoning is
229 visible, it show two distinct textures: regular and patchy (Figs. 3, 4 and 5; Table 5). The term

https://doi.org/10.5194/se-2019-162
Preprint. Discussion started: 30 October 2019

regular refers to crystals showing growth-zonation, whereas a patchy texture indicates monazite replacement by secondary through dissolution/reprecipitation processes (e.g. Ayers et al., 1999; Bergemann et al., 2018, 2019b, 2019a; Gnos et al., 2015). Thorium and U contents of the dated fissure monazites display a large variability, ranging between ~50 to 64,000 ppm Th and ~1 to 1000 ppm U, with variations in Th/U ratio from 1 up to ~7000 (Figs. 3, 4 and 5; Tables 3 and 4). ^{232}Th-^{208}Pb ages presented on the right-hand panel of figures 3, 4 and 5 are arranged according to the order established in tables 3 and 4. A detailed description of each monazite grain is provided in the Supplementary Information. Average ages are reported for group of dates on texturally and/or chemically similar domains. In order to ensure that a group of dates from a domain is internally consistent, rare outliers have been excluded to bring the MSWD within acceptable values (Spencer et al., 2016). In a few cases it remains that the date for a specific monazite domains have a scatter above analytical uncertainty (e.g. grain 6, 9, 24), which probably reflects the complex formation process of fissure monazite.

The investigated grains from the western part of the western Tauern sub-dome come from the Venediger Duplex, with the exception of sample 6, which comes from the Glockner Nappe System (Fig. 1; Table 1). The samples 2, 4 and 6 were collected near to the major Brenner normal fault, which delimits the western limb of the TW, and samples 1, 3, 5 and 7 were collected in the vicinity of sinistral strike-slip faults (Fig. 1). Average growth domain ages range from 20.8 ± 0.6 to 7.7 ± 0.9 Ma (samples 3 and 2) with the youngest ages recorded in the western TW (Figs. 1, 3 and 6a; Tables 3, 4 and 5).

The central part of the TW displays growth domain ages between 18.3 ± 1.2 to 10.3 ± 0.2 (samples 12 and 14; Figs. 1 and 4; Tables 3, 4 and 5), but the majority of the dated monazites in

https://doi.org/10.5194/se-2019-162
Preprint. Discussion started: 30 October 2019

this area record ages around 17 Ma (Fig. 6b). Samples 8, 9 and 10 were collected between the eastern and western termination of the ASZ and the SEMP fault (Fig. 1). Another three samples (11, 12 and 13; Table 1) were collected in the northern prolongation of the AhSZ and a seventh monazite (grain 14) was sampled near the southern border of the eastern part of the western sub-dome (Fig. 1).

The oldest ages are principally recorded in the eastern part of the TW at around 21 Ma (Fig. 6c). Average ages of growth domains range from 22.3 ± 0.6 to 17.3 ± 1.2 Ma (samples 20 and 25; Figs. 1, 4 and 6c; Tables 3, 4 and 5). The samples were mainly collected at the western border of the eastern sub-dome, in the Venediger Duplex or near the boundary with the Glockner/ Modereck Nappe Systems (Fig. 1). Sample 25 was taken at some distance from the other samples, near the south-eastern border of the eastern sub-dome (Fig. 1).

5 Discussion

5.1 Fissure monazite ages

The oldest monazite ages of 22.3 ± 0.6 to 20.1 ± 0.3 Ma (found in samples 20 and 18; Figs. 1, 6c and 7a and d) are common in the eastern Tauern, but can also be found in the western area (Fig. 7a, c and d, red symbols). This in line with regional fault activity recorded at ca. 21 Ma based on Pleuger et al. (2012) (Fig. 8a) which corresponds to the main indentation phase (Favaro et al., 2017). We interpret these as a first monazite crystallization during E-W extension in association with the dome formation (N-S shortening) when the existing clefts reached P-T conditions at which fissure monazite starts to grow (phase (1) on figure 7). When comparing an assumed fissure formation temperature of 450°C (typically obtained in quartz fluid inclusion studies on

https://doi.org/10.5194/se-2019-162
Preprint. Discussion started: 30 October 2019

early alpine fissures, (e.g., Mullis, 1996)) with thermochronological data of the eastern TW (compiled in Wölfler et al. 2012), the onset of fissure formation, predating primary monazite crystallization, is estimated at around 25 Ma. Based on a comparison with thermochronological data, monazite crystallization recorded between 19 – 15 Ma was estimated to have occurred at ~300 - 200°C in the eastern TW (Gnos et al., 2015). New monazite ages from this study in the eastern TW are up to ~22 Ma (sample 20), suggesting that early monazite crystallization in the area may have occurred at higher temperatures of 400 – 350°C.

While early fissure formation is related to E-W extension (leading to flat foliation and E-W mineral lineations; Fig. 2c), we suggest that monazite formation also occurred along the sinistral strike-slip to oblique-slip movements (vertical foliation and flat to inclined lineation; Fig. 2), particularly developed in the central and western part of the TW (e.g. Rosenberg et al., 2018; Schneider et al., 2013). These shear zones developed as a result of bending of the E-W oriented upright folds around a vertical axis (leading edge of the Dolomite indenter) (Fig. 1). This occurred when N-S shortening could no longer be accommodated by folding and doming within the TW. Associated with these movements is the formation of a younger generation of fissures (see Pfitscherjoch example above) which peak activity is recorded at ca. 17 Ma (phase (2), green symbols on figure 7). This fissure generation is associated with steep foliation and flat lineation (Fig. 2), but sub-parallel in orientation to the earlier fissure formation. The monazite ages at ~17 Ma are mainly found in the western and central TW (Figs. 1, 6 and 7; samples 5, 8, 10, 11, 12 and 13 respectively; Table 5), in association with sinistral fault zones, as in the Pfitscherjoch region or near the eastern termination of the ASZ and AhSZ faults (see above). Unfortunately, we do not have structural information on the westernmost and easternmost analysed samples (6 and 25; Figs 1, 6 and 7), but they can be speculated to also have formed in association with a strike slip shear zone or the BNF in the case of sample 6. At larger scale, these movements seem to have been

https://doi.org/10.5194/se-2019-162
Preprint. Discussion started: 30 October 2019

299 associated with the development of the sinistral Giudicarie Fault (GF, located at the southwestern
300 corner of the TW), offsetting the Periadriatic Fault (PF; Fig. 8b, e.g., Pleuger et al., 2012). Ages
301 of ca. 17 Ma are also recorded in the eastern part of the TW, likely linked to the KNF and Mölltal
302 Fault (MöF) activity (samples 16, 17, 21 and 25; Fig. 7a and d; e.g. Favaro et al., 2017). In grains
303 from near the MVF (e.g. Kurz and Neubauer, 1996), the dextral shear zone at the boundary
304 between the Penninic and Subpenninic nappes at the south-eastern limit of the TW (Fig. 1),
305 numerous monazite growth domains yield ages between 15.6 ± 0.7 and 15.0 ± 0.5 Ma (bracketed
306 by samples 22 and 21 from Gnos et al., 2015; Figs 1, 6c, 7a and d; green circles on figure 7d;
307 Table 5). These ages date the latest known activity of this sinistral shear zone to ~15 Ma.
308 Whereas younger ages, associated with reactivation of fault zones are widespread in the central
309 and western TW, tectonic movements seem to cease in the eastern TW after this time (Fig. 8c).

310 The youngest monazite growth domain ages, ranging from 13.1 ± 0.3 to 7.7 ± 0.9 Ma (samples 5
311 and 2; Table 5), indicate steps of reactivation of the different sinistral strike-slip to oblique-slip
312 movements along different faults (phase (3) and blue symbols on figure 7). Based on our
313 monazite crystallization data, the oldest activities of this younger phase are recorded near the
314 AhSZ and GSZ (samples 5 and 7). The youngest activities are recorded in association with the
315 ASZ, OSZ and TSZ on figure 7a-c; samples 1, 2 and 4), and in the central TW in an area located
316 south of the main fault systems (sample 14, Figure 7a). In addition to faults activity at ca. 12 Ma
317 (Fig. 8), coeval strike-slip activity has also been documented in many areas of the central and
318 western Alps (e.g., Bergemann et al., 2017, 2019b; Berger et al., 2013; Gasquet et al., 2010;
319 Grand'Homme et al., 2016a; Pleuger et al., 2012; Ricchi et al., 2019).

320 In summary, in the western TW, monazite ages constrain the activities of the ASZ (18 – 12 Ma),
321 AhSZ (18 – 13 Ma), TSZ/OSZ (12 – 8 Ma; older ages of sample 3 (Fig. 7) are probably related to

https://doi.org/10.5194/se-2019-162
Preprint. Discussion started: 30 October 2019

322 extensional unroofing) and GSZ (17 – 13 Ma). In the eastern part, the MVF is active between 19
323 and 15 Ma.

324

325 **5.2 Comparison with shear zone dating**

326 A number of attempts to date shear zone activity in the TW using Ar-Ar, Rb-Sr and Sm-Nd
327 techniques have been made in the past, which were, however, based on mineral separation
328 techniques without a clear structural control on the dated grains (e.g., Blanckenburg et al., 1989;
329 Glodny et al., 2008; Pollington and Baxter, 2010, 2011; Urbanek et al., 2002). An exception to
330 this is the $^{40}Ar/^{39}Ar$ study of Schneider et al. (2013) on syn-kinematic phengite and K-feldspar
331 which will be used in the following as a comparison (Table 2). Fissure monazite ages largely
332 corroborate this work, similarly showing the longevity of different shear zones in the TW. The
333 ages confirm that even though most of the dated monazite samples are only located in the damage
334 zone in the vicinity of the core of the shear zones, fluid-filled fissures provide a sensitive system
335 where tectonic activity triggers fluid-enhanced dissolution/precipitation reactions at lower
336 greenschist to sub-greenschist facies conditions.

337 While Schneider et al. (2013) obtained crystallization age ranges of 33 - 15 Ma for the ASZ, 24 -
338 12 Ma for the TSZ and 20 - 7 Ma for the GSZ (Table 2), our data confirms activity at 18 – 12, 12
339 – 8 and 17 – 13 Ma respectively (Fig. 7). The data presented here indicate that all of the shear
340 zones where active until ~13 – 12 Ma, and the Tuxer and/or Olperer shear zones even until ~8
341 Ma. However, the fissure monazite data does not date the initiation of the GSZ (Selverstone et al.,
342 1991), nor the earliest activity of the TSZ (greenschist to amphibolite facies; Selverstone et al.,
343 1984, 1991) or the ASZ (greenschist facies; Cole et al., 2007), since their formation already
344 occurred at amphibolite facies conditions. As Alpine fissures only form under greenschist facies

https://doi.org/10.5194/se-2019-162
Preprint. Discussion started: 30 October 2019

345 conditions, the oldest monazite crystallization ages are younger than the data obtained by
346 Schneider et al. (2013). This indicates that shear zone activity started earlier than the fissure
347 monazite record. As the monazite age range of the younger fault activity is comparable to the
348 data of Schneider et al. (2013), but is not the same for individual shear zones, it seems likely that
349 all shear zones of the western TW were active as recently as 8 - 7 Ma.

350

351 **5.3 Comparison with fission track data**

352 There is a wealth of zircon fission track (ZFT) data (Bertrand et al., 2013, 2017; Dunkl et al.,
353 2003 ; Fügenschuh et al., 1997 ; Mancktelow et al., 2001 ; Most, 2003 ; Pomella, 2010 ; Steenken
354 et al., 2002 ; Stöckhert et al., 1999 ; Viola et al., 2001 ; Wölfler et al., 2008) and apatite fission
355 track (AFT) data (Bertrand et al., 2013, 2017 ; Coyle, 1994 ; Di Fiore, 2013 ; Foeken et al., 2007
356 ; Fügenschuh et al., 1997 ; Grundmann and Morteani, 1985 ; Hejl, 1997 ; Mancktelow et al.,
357 2001 ; Most, 2003 ; Pomella, 2010 ; Staufenberg, 1987, Steenken et al., 2002 ; Viola et al., 2001 ;
358 Wölfler et al., 2008, 2012) that can assist in describing the exhumation and low grade tectonic
359 activity in the TW.
360 Three cross sections, DD' (perpendicular to the BNF), AA' (perpendicular to the western limb of
361 the western subdome) and EE' (parallel to the main axial plane of the TW) are presented in figure
362 7, redrawn after Bertrand et al. (2017) and Schmid et al. (2013). Zircon and apatite fission track
363 data compiled by Bertrand et al. (2017) are displayed in the lower part of figure 7b-d and
364 compared to fissure monazite ages. As described in Bertrand et al. (2017) (first model), fission
365 tracks data along AA' cross section (Fig. 7c) nicely display a dome-like shape with younger ages
366 recorded near the sub-dome axial plane, were cooling was slower. Whereas along the EE'
367 longitudinal cross section (Fig. 7d), ZFT and AFT are younger in the western and eastern border

https://doi.org/10.5194/se-2019-162
Preprint. Discussion started: 30 October 2019

368 of the TW where the two major extensional faults, the BNF and KNF, are respectively located.
369 Perpendicular to the BNF (DD' cross section, Fig. 7b), the fission tracks record cooling ages
370 younging from the footwall toward the plane of the normal fault (from 10 to 4 Ma for AFT;
371 second model of Bertrand et al. 2017). The youngest monazite ages (15 – 8 Ma) lie between
372 zircon and apatite fission track data (grey and blue symbols), whereas the older ages (>17 Ma,
373 red and green symbols) do not follow the cooling trend and are equal to or older than the ZFT
374 data. This means that at least the fissure monazite recording older ages crystallized somewhere
375 above ZFT closure temperatures of ca. 280–240 °C (Bernet, 2009; Bernet and Garver, 2005;
376 Reiners, 2005; Yamada et al., 1995) (Fig. 7d).
377

378 **5.4 Monazite Th/U as monitor of oxidizing and reducing conditions**

379 Extreme low and high Th/U ratios described in fissure monazite by Gnos et al. 2015 (T1, T2 and
380 T3 sample in figure 9) are also observed in some grains from this study (red and blue labels on
381 figure 9). Hydrothermal monazite from the TW associated with hematite in fissure typically
382 displays very high Th/U ratios of around 1200 (Fig. 9, red labels; Table 1), whereas grains
383 obtained from graphite-bearing host rocks show very low Th/U ratios around 8 (Fig. 9, blue
384 labels; Table 1). This respectively attests for oxidizing and reducing fluid conditions in the fissure
385 environment.

386 The Th/U in monazite grains PFIT1 and MOKR1 would instead record a dynamic oxidation
387 environment due to variable fluid conditions. In PFIT1 monazite the Th/U decreases from core to
388 rim decreases, whereas within MOKR1 the opposite evolution is observed (Fig. 9). Thus in the
389 first case the fissure environment evolves toward reducing conditions whereas in the second case
390 there is an evolution towards more oxidizing conditions. Many of the other grains indicate

https://doi.org/10.5194/se-2019-162
Preprint. Discussion started: 30 October 2019

391 intermediate oxidizing conditions and they could not be assigned to one of the two categories
392 defined above, as the presence of either hematite or graphite is uncertain (Fig. 9; grey labels).

393

394 **6 Conclusions**

395 Th-Pb ages of fissure monazite provides an extended record of exhumation of the TW during
396 Miocene. The investigated monazites crystallized at temperatures <400°C in the presence of
397 hydrothermal fluids that circulated in open fissures formed through tectonic movements. The Th-
398 Pb ages recorded by fissure monazites are in general agreement with previously published
399 geochronological data and range between 22.3 ± 0.6 Ma and 7.7 ± 0.9 Ma. The oldest spot dates
400 are recorded around 25 Ma, meaning that monazite crystallization in the metamorphic and
401 structural Tauern dome occurred over a period of ~17 Ma. The combination of structural and
402 geochronological information allows relating monazite growth with tectonic movements that
403 affected the TW. The three major growth episodes identified in this study are interpreted to be
404 related to N-S shortening associated to E-W extension (22 – 19 Ma), contemporaneous N-S
405 shortening and sinistral strike-slip movements (19 – 15 Ma) and reactivation of strike-
406 slips/normal faulting (13 – 8 Ma). Overall, Cenozoic faults were active around the TW at 21, 17
407 and 12 Ma. Comparison of Th-Pb fissure monazite crystallization ages with existing
408 crystallization and cooling ages (e.g. AFT, ZFT, white mica from fault zones) shows that
409 monazite crystallization ages do not show the U-shaped distribution as cooling ages, when
410 plotted on a section perpendicular to the main fold axis of the Tauern window (Fig. 7). This
411 enlarged dataset also supports previous observations on fissure monazites chemistry displaying
412 extremely high Th/U ratios (ca. 1200) under oxidizing conditions in association with hematite
413 (Fig. 9).

https://doi.org/10.5194/se-2019-162
Preprint. Discussion started: 30 October 2019

414 *Data availability.* The data used in this study are available in Tables 3 and 4.

415 *Author contributions.* Fissure monazite samples were organized by EG and FW. Monazite for
416 dating were selected by ER, CAB, EG and AB according to tectonic setting and fault activity of
417 the study area. ER prepared the manuscript during her PhD project under the supervision of EG,
418 with contributions from all co-authors. Sample preparation and BSE imaging was performed by
419 ER and CAB. Data acquisition and reduction at the SwissSIMS and NordSim facility was
420 respectively carried out by ER and CAB under the supervision of DR and MJW.

421 *Competing interests*. The authors declare that they have no conflict of interest.

422 *Acknowledgments.* We thank Sepp Brugger, Kurt Novak, Franz Gartner, Peter Hellweger, Adolf
423 Meyer, Sebastian Plankensteiner, Johann Rappold, Josef Rathgeb, Alexandre Salzmann, Maria
424 Schaffhauser, Andreas Steiner and Ermin Welzl for having provided samples for this study. This
425 study was financed by the SNF grant number 200020-165513.

426

427 **References**

428 Aleinikoff, J. N., Schenck, W. S., Plank, M. O., Srogi, L. A., Fanning, C. M., Kamo, S. L. and
429 Bosbyshell, H.: Deciphering igneous and metamorphic events in high-grade rocks of the
430 Wilmington complex, Delaware: Morphology, cathodoluminescence and backscattered electron
431 zoning, and SHRIMP U-Pb geochronology of zircon and monazite, Bull. Geol. Soc. Am., 118(1–
432 2), 39–64, doi:10.1130/B25659.1, 2006.

433 Ayers, J. C., Miller, C., Gorisch, B. and Milleman, J.: Textural development of monazite during
434 high-grade metamorphism: Hydrothermal growth kinetics, with implications for U,Th-Pb

https://doi.org/10.5194/se-2019-162
Preprint. Discussion started: 30 October 2019

435 geochronology, Am. Mineral., 84(11–12), 1766–1780, doi:10.2138/am-1999-11-1206, 1999.

436 Bergemann, C. A., Gnos, E., Berger, A., Whitehouse, M., Mullis, J., Wehrens, P., Pettke, T. and
437 Janots, E.: Th-Pb ion probe dating of zoned hydrothermal monazite and its implications for
438 repeated shear zone activity: An example from the Central Alps, Switzerland, Tectonics, 36(4),
439 671–689, doi:10.1002/2016TC004407, 2017.

440 Bergemann, C. A., Gnos, E., Berger, A., Whitehouse, M. J., Mullis, J., Walter, F. and Bojar, H. P.:
441 Constraining long-term fault activity in the brittle domain through in situ dating of hydrothermal
442 monazite, Terra Nov., 30(6), 440–446, doi:10.1111/ter.12360, 2018.

443 Bergemann, C. A., Gnos, E., Berger, A., Janots, E. and Whitehouse, M. J.: Constraining
444 metamorphic dome exhumation and fault activity through hydrothermal monazite-(Ce), ,
445 (February), 1–23, 2019a.

446 Bergemann, C. A., Gnos, E. and Whitehouse, M. J.: Insights into the tectonic history of the
447 Western Alps through dating of fi ssure monazite in the Mont Blanc and Aiguilles Rouges
448 Massifs, Tectonophysics, 750(May 2018), 203–212, doi:10.1016/j.tecto.2018.11.013, 2019b.

449 Berger, A., Gnos, E., Janots, E., Whitehouse, M., Soom, M., Frei, R. and Waight, T. E.: Dating
450 brittle tectonic movements with cleft monazite: Fluid-rock interaction and formation of REE
451 minerals, Tectonics, 32(5), 1176–1189, doi:10.1002/tect.20071, 2013.

452 Bernet, M.: A fi eld-based estimate of the zircon fi ssion-track closure temperature, , 259, 181–
453 189, doi:10.1016/j.chemgeo.2008.10.043, 2009.

454 Bernet, M. and Garver, J. I.: Fission-track analysis of detrital zircon, Rev. Mineral. Geochemistry,
455 58.1, 205–237, 2005.

https://doi.org/10.5194/se-2019-162
Preprint. Discussion started: 30 October 2019

456 Bertrand, A.: Exhuming the core of collisional orogens, the Tauern Window (Eastern-Alps) A
457 geochronological, modelling and structural study, , 175, 2013.

458 Bertrand, A., Rosenberg, C. and Garcia, S.: Fault slip analysis and late exhumation of the Tauern
459 Window, Eastern Alps, Tectonophysics, 649, 1–17, doi:10.1016/j.tecto.2015.01.002, 2015.

460 Bertrand, A., Rosenberg, C., Rabaute, A., Herman, F. and Fügenschuh, B.: Exhumation
461 mechanisms of the Tauern Window (Eastern Alps) inferred from apatite and zircon fission track
462 thermochronology, Tectonics, 36(2), 207–228, doi:10.1002/2016TC004133, 2017.

463 Blanckenburg, F. v., Villa, I. M., Baur, H., Morteani, G. and Steiger, R. H.: Time calibration of a
464 PT-path from the Western Tauern Window, Eastern Alps: the problem of closure temperatures,
465 Contrib. to Mineral. Petrol., 101(1), 1–11, doi:10.1007/BF00387196, 1989.

466 Cherniak, D. J., Watson, E. B., Grove, M. and Harrison, T. M.: Pb diffusion in monazite: A
467 combined RBS/SIMS study, Geochim. Cosmochim. Acta, 68(4), 829–840,
468 doi:10.1016/j.gca.2003.07.012, 2004.

469 Cole, J., Hacker, B., Ratschbacher, L., Dolan, J., Seward, G., Frost, E. and Frank, W.: Localized
470 ductile shear below the seismogenic zone: Structural analysis of an exhumed strike-slip fault,
471 Austrian Alps, J. Geophys. Res. Solid Earth, 112(12), 1–15, doi:10.1029/2007JB004975, 2007.

472 Coyle, D. A.: The application of apatite fission-track analysis to problem in tectonics, PhD thesis,
473 La Trobe Univ. Bundoora, Victoria, Australia., 1994.

474 Dunkl, I., Frisch, W. and Grundmann, G.: Zircon fission-track thermochronology of the south-
475 eastern part of the TW and the adjacent Austroalpine margin, Eastern Alps, Eclogae Geol. Helv.,
476 96, 209–217, doi:10.1007/s00015-003-1092-3, 2003.

https://doi.org/10.5194/se-2019-162
Preprint. Discussion started: 30 October 2019

477 Favaro, S., Handy, M. R., Scharf, A. and Schuster, R.: Changing patterns of exhumation and
478 denudation in front of an advancing crustal indenter, Tauern Window (Eastern Alps), Tectonics,
479 36(6), 1053–1071, doi:10.1002/2016TC004448, 2017.

480 Di Fiore, G.: Evoluzione Morfotettonica delle aree alpine “Sempione” e “Brennero” attraverso
481 studi termocronologici di bassa temperatura, PhD thesis, Università di Bologna., 2013.

482 Fitz-Diaz, E., Cottle, J. M., Vidal-Reyes, M. I. and van der Pluijm, B.: In situ Th/Pb dating of
483 monazite in fibrous veins: Direct dating of veins and deformation in the shallow upper crust of
484 the Mexican Orogen, J. Struct. Geol., 124(April), 136–142, doi:10.1016/j.jsg.2019.04.004, 2019.

485 Foeken, J. P. T., Persano, C., Stuart, F. M. and ter Voorde, M.: Role of topography in isotherm
486 perturbation: Apatite (U-Th)/He and fission track results from the Malta tunnel, Tauern Window,
487 Austria, Tectonics, 26(3), doi:10.1029/2006TC002049, 2007.

488 Fügenschuh, B., Seward, D. and Mancktelow, N.: Exhumation in a convergent orogen: the
489 western Tauern Window, Terra Nov., 9(5–6), 213–217, doi:10.1111/j.1365-3121.1997.tb00015.x,
490 1997.

491 Gardés, E., Jaoul, O., Montel, J. M., Seydoux-Guillaume, A. M. and Wirth, R.: Pb diffusion in
492 monazite: An experimental study of Pb2 + + Th4 + ??? 2 Nd3 + interdiffusion, Geochim.
493 Cosmochim. Acta, 70(9), 2325–2336, doi:10.1016/j.gca.2006.01.018, 2006.

494 Gardés, E., Montel, J. M., Seydoux-Guillaume, A. M. and Wirth, R.: Pb diffusion in monazite:
495 New constraints from the experimental study of Pb2 + □ Ca2 + interdiffusion, Geochim.
496 Cosmochim. Acta, 71(16), 4036–4043, doi:10.1016/j.gca.2007.06.036, 2007.

497 Gasquet, D., Bertrand, J. M., Paquette, J. L., Lehmann, J., Ratzov, G., Ascenção De Guedes, R.
498 A., Tiepolo, M., Boullier, A. M., Scaillet, S. and Nomade, S.: Miocene to Messinian deformation

https://doi.org/10.5194/se-2019-162
Preprint. Discussion started: 30 October 2019

499 and hydrothermal activity in a pre-Alpine basement massif of the French western Alps: New U-
500 Th-Pb and argon ages from the Lauzière massif, Bull. la Soc. Geol. Fr., 181(3), 227–241,
501 doi:10.2113/gssgfbull.181.3.227, 2010.

502 Glodny, J., Ring, U. and Kühn, A.: Coeval high-pressure metamorphism, thrusting, strike-slip,
503 and extensional shearing in the Tauern Window, Eastern Alps, Tectonics, 27(4),
504 doi:10.1029/2007TC002193, 2008.

505 Glotzbach, C., Reinecker, J., Danišík, M., Rahn, M., Frisch, W. and Spiegel, C.: Thermal history
506 of the central Gotthard and Aar massifs, European Alps: Evidence for steady state, long-term
507 exhumation, J. Geophys. Res. Earth Surf., 115(3), F03017, doi:10.1029/2009JF001304, 2010.

508 Gnos, E., Janots, E., Berger, A., Whitehouse, M., Walter, F., Pettke, T. and Bergemann, C.: Age of
509 cleft monazites in the eastern Tauern Window: constraints on crystallization conditions of
510 hydrothermal monazite, Swiss J. Geosci., 108(1), 55–74, doi:10.1007/s00015-015-0178-z, 2015.

511 Grand'Homme, A., Janots, E., Bosse, V., Seydoux-Guillaume, A. M. and Ascenção De Guedes,
512 R. A.: Interpretation of U-Th-Pb in-situ ages of hydrothermal monazite-(Ce) and xenotime-(Y):
513 evidence from a large-scale regional study in clefts from the western alps, Mineral. Petrol.,
514 110(6), 787–807, doi:10.1007/s00710-016-0451-5, 2016a.

515 Grand'Homme, A., Janots, E., Seydoux-Guillaume, A. M., Guillaume, D., Bosse, V. and Magnin,
516 V.: Partial resetting of the U-Th-Pb systems in experimentally altered monazite: Nanoscale
517 evidence of incomplete replacement, Geology, 44(6), 431–434, doi:10.1130/G37770.1, 2016b.

518 Grand'Homme, A., Janots, E., Seydoux-Guillaume, A. M., Guillaume, D., Magnin, V.,
519 Hövelmann, J., Höschen, C. and Boiron, M. C.: Mass transport and fractionation during monazite
520 alteration by anisotropic replacement, Chem. Geol., 484(October 2017), 51–68,

https://doi.org/10.5194/se-2019-162
Preprint. Discussion started: 30 October 2019

521 doi:10.1016/j.chemgeo.2017.10.008, 2018.

522 Grundmann, G. and Morteani, G.: The young uplift and thermal history of the central Eastern
523 Alps (Austria/Italy), evidence from apatite fission track ages, Jahrb. Geol. Bundesanst, 128, 197–
524 216, 1985.

525 Hejl, E.: "Cold spots" during the Cenozoic evolution of the Eastern Alps: Thermochronological
526 interpretation of apatite fission-track data, Tectonophysics, 272(2–4), 159–173,
527 doi:10.1016/S0040-1951(96)00256-9, 1997.

528 Janots, E., Berger, A., Gnos, E., Whitehouse, M., Lewin, E. and Pettke, T.: Constraints on fluid
529 evolution during metamorphism from U–Th–Pb systematics in Alpine hydrothermal monazite,
530 Chem. Geol., 326, 61–71, 2012.

531 Janots, E., Homme, A. G., Bernet, M., Guillaume, D. and Gnos, E.: Geochronological and
532 thermometric evidence of unusually hot fluids in an Alpine fissure of Lauzière granite
533 (Belledonne, Western Alps), , 211–223, 2019.

534 Kurz, W. and Neubauer, F.: Deformation partitioning during updoming of the Sonnblick area in
535 the Tauern Window (Eastern Alps, Austria), J. Struct. Geol., 18(11), 1327–1337,
536 doi:10.1016/S0191-8141(96)00057-0, 1996.

537 Ludwig, K. R.: User's manual for a geochronological toolkit for Microsoft Excel (Isoplot/Ex
538 version 3.0), Berkeley Geochronol. Cent. Spec. Publ., 4, 1–70, 2003.

539 Ludwig, K. R.: Squid2: a user manual., Berkeley Geochronol. Cent. Spec. Publ., 5, 1–110, 2009.

540 Luth, S. W. and Willingshofer, E.: Mapping of the post-collisional cooling history of the Eastern
541 Alps, Swiss J. Geosci., 101(SUPPL. 1), doi:10.1007/s00015-008-1294-9, 2008.

https://doi.org/10.5194/se-2019-162
Preprint. Discussion started: 30 October 2019

542 Mancktelow, N. S., Stöckli, D. F., Grollimund, B., Müller, W., Fügenschuh, B., Viola, G.,
543 Seward, D. and Villa, I. M.: The DAV and Pediatriatic fault systems in the Eastern Alps South of
544 the Tauern window, Int. J. Earth Sci., 90(3), 593–622, doi:10.1007/s005310000190, 2001.

545 Most, P.: Late Alpine cooling histories of tectonic blocks along the central part of the Transalp-
546 Traverse (Inntal-Gadertal): Constraints from geochronology, PhD thesis, p. 97, Univ. of
547 Tübingen., 2003.

548 Mullis, J.: P-T-t path of quartz formation in extensional veins of the Central Alps, Schweiz.
549 Miner. Petrogr. Mitt, 76, 159–164, doi:10.5169/seals-57694, 1996.

550 Pleuger, J., Mancktelow, N., Zwingmann, H. and Manser, M.: K-Ar dating of synkinematic clay
551 gouges from Neoalpine faults of the Central, Western and Eastern Alps, Tectonophysics, 550–
552 553, 1–16, doi:10.1016/j.tecto.2012.05.001, 2012.

553 Pollington, A. D. and Baxter, E. F.: High resolution Sm-Nd garnet geochronology reveals the
554 uneven pace of tectonometamorphic processes, Earth Planet. Sci. Lett., 293(1–2), 63–71,
555 doi:10.1016/j.epsl.2010.02.019, 2010.

556 Pollington, A. D. and Baxter, E. F.: High precision microsampling and preparation of zoned
557 garnet porphyroblasts for Sm-Nd geochronology, Chem. Geol., 281(3–4), 270–282,
558 doi:10.1016/j.chemgeo.2010.12.014, 2011.

559 Pomella, H.: The Cenozoic evolution of the Giudicarie fault system (Eastern/Southern Alps,
560 northern Italy). A geochronological, structural and paleomagnetic study, PhD thesis, Institute of
561 Geology and Paleontology, Univ. of Innsbruck., 2010.

562 Putnis, A.: Mineral Replacement Reactions, Rev. Miner. Geochem., 70.1, 87–124,
563 doi:10.2138/rmg.2009.70.3, 2009.

https://doi.org/10.5194/se-2019-162
Preprint. Discussion started: 30 October 2019

564 Reiners, P. W.: Zircon (U-Th)/He Thermochronometry, in Reviews in Mineralogy and
565 Geochemistry, vol. 58, edited by T. A. Reiners, P.W. and Ehlers, pp. 151–179., 2005.

566 Ricchi, E., Bergemann, C. A., Gnos, E., Berger, A., Rubatto, D. and Whitehouse, M. J.:
567 Constraining deformation phases in the Aar Massif and the Gotthard Nappe (Switzerland) using
568 ThPb crystallization ages of fissure monazite-(Ce), Lithos, 2019.

569 Rosenberg, C. L. and Berger, A.: On the causes and modes of exhumation and lateral growth of
570 the Alps, Tectonics, 28(6), doi:10.1029/2008TC002442, 2009.

571 Rosenberg, C. L. and Garcia, S.: Estimating displacement along the Brenner Fault and orogen-
572 parallel extension in the Eastern Alps, Int. J. Earth Sci., 100(5), 1129–1145, doi:10.1007/s00531-
573 011-0645-3, 2011.

574 Rosenberg, C. L., Schneider, S., Scharf, A., Bertrand, A., Hammerschmidt, K., Rabaute, A. and
575 Brun, J. P.: Relating collisional kinematics to exhumation processes in the Eastern Alps, Earth-
576 Science Rev., 176(March 2017), 311–344, doi:10.1016/j.earscirev.2017.10.013, 2018.

577 Scharf, A., Handy, M. R., Favaro, S., Schmid, S. M. and Bertrand, A.: Modes of orogen-parallel
578 stretching and extensional exhumation in response to microplate indentation and roll-back
579 subduction (Tauern Window, Eastern Alps), Int. J. Earth Sci., 102(6), 1627–1654,
580 doi:10.1007/s00531-013-0894-4, 2013.

581 Schmid, S. M., Fügenschuh, B., Kissling, E. and Schuster, R.: Tectonic map and overall
582 architecture of the Alpine orogen, Eclogae Geol. Helv., 97(1), 93–117, doi:10.1007/s00015-004-
583 1113-x, 2004.

584 Schmid, S. M., Scharf, A., Handy, M. R. and Rosenberg, C. L.: The Tauern Window (Eastern
585 Alps , Austria): a new tectonic map , with cross-sections and a tectonometamorphic synthesis, ,

https://doi.org/10.5194/se-2019-162
Preprint. Discussion started: 30 October 2019

586 1–32, doi:10.1007/s00015-013-0123-y, 2013.

587 Schmidt, C.: Evolution of the Eastern Alps, , 1–13, 2013.

588 Schneider, S., Hammerschmidt, K. and Rosenberg, C. L.: Dating the longevity of ductile shear
589 zones: Insight from 40Ar/39Ar in situ analyses, Earth Planet. Sci. Lett., 369–370(May 2012), 43–
590 58, doi:10.1016/j.epsl.2013.03.002, 2013.

591 Selverstone, J.: Evidence for east-west crustal extension in the Eastern Alps: Implications for the
592 unroofing history of the Tauern Window, Tectonics, 7(1), 87–105, 1988.

593 Selverstone, J., Spear, F. S., Franz, G. and Morteani, G.: High-pressure metamorphism in the SW
594 tauern window, Austria: P-T paths from hornblende-kyanite-staurolite schists, J. Petrol., 25(2),
595 501–531, doi:10.1093/petrology/25.2.501, 1984.

596 Selverstone, J., Morteani, G. and Staude J.-M: Fluid channelling during ductile shearing:
597 transformation of granodiorite into aluminous schist in the Tauern Window, Eastern Alps, J.
598 Metamorph. Geol., 9(4), 419–431, 1991.

599 Seydoux-Guillaume, A. M., Montel, J. M., Bingen, B., Bosse, V., de Parseval, P., Paquette, J. L.,
600 Janots, E. and Wirth, R.: Low-temperature alteration of monazite: Fluid mediated coupled
601 dissolution-precipitation, irradiation damage, and disturbance of the U-Pb and Th-Pb
602 chronometers, Chem. Geol., 330–331, 140–158, doi:10.1016/j.chemgeo.2012.07.031, 2012.

603 Spencer, C. J., Kirkland, C. L. and Taylor, R. J. M.: Geoscience Frontiers Strategies towards
604 statistically robust interpretations of in situ U e Pb zircon geochronology, Geosci. Front., 7(4),
605 581–589, doi:10.1016/j.gsf.2015.11.006, 2016.

606 Stacey, J. S., and Kramers, J. D.: Approximation of terrestrial lead isotope evolution by a two-

https://doi.org/10.5194/se-2019-162
Preprint. Discussion started: 30 October 2019

607 staged model, Earth Planet. Sci. Lett., 26, 207–221, 1975.

608 Staufenberg, H.: Apatite fission-track evidence for postmetamorphic uplift and cooling history of
609 the Eastern Tauern Window and the surrounding Austroalpine (Central Eastern Alps, Austria),
610 Jahrb. Geol. Bundesanst, 130(1985), 571–586 [online] Available from:
611 http://www.landesmuseum.at/pdf_frei_remote/JbGeolReichsanst_130_0571.pdf%5Cnpapers3://p
612 ublication/uuid/A492C816-3706-4ACB-9EE2-44E4AEB00320, 1987.

613 Steenken, A., Siegesmund, S., Heinrichs, T. and Fügenschuh, B.: Cooling and exhumation of the
614 Rieserferner Pluton (Eastern Alps, Italy/Austria), Int. J. Earth Sci., 91(5), 799–817,
615 doi:10.1007/s00531-002-0260-4, 2002.

616 Stöckhert, B., Brix, M. R., Kleinschrodt, R., Hurford, A. J. and Wirth, R.: Thermochronometry
617 and microstructures of quartz-a comparison with experimental flow laws and predictions on the
618 temperature of the brittle-plastic transition, J. Struct. Geol., 21(3), 351–369, doi:10.1016/S0191-
619 8141(98)00114-X, 1999.

620 Urbanek, C., Frank, W., Grasemann, B. and Decker, K.: Eoalpine versus Tertiary deformation:
621 dating of heterogeneously partitioned strain (Tauern Window, Austria), in Abstract volume, edited
622 by PanGeo Austria., 2002.

623 Viola, G., Mancktelow, N. S. and Seward, D.: Late oligocene-neogene evolution of Europe-Adria
624 collision: New structural and geochronological evidence from the Giudicarie fault system (Italian
625 Eastern Alps), Tectonics, 20(6), 999–1020, doi:10.1029/2001TC900021, 2001.

626 Wölfler, A., Dekant, C., Danišík, M., Kurz, W., Dunkl, I., Putiš, M. and Frisch, W.: Late stage
627 differential exhumation of crustal blocks in the central Eastern Alps: Evidence from fission track
628 and (U-Th)/He thermochronology, Terra Nov., 20(5), 378–384, doi:10.1111/j.1365-

https://doi.org/10.5194/se-2019-162
Preprint. Discussion started: 30 October 2019

3121.2008.00831.x, 2008.

Wölfler, A., Stüwe, K., Danišík, M. and Evans, N. J.: Low temperature thermochronology in the Eastern Alps: Implications for structural and topographic evolution, Tectonophysics, 541–543, 1–18, doi:10.1016/j.tecto.2012.03.016, 2012.

Yamada, R., Tagami, T., Nishimura, S. and Ito, H.: Chemical Annealing kinetics of fission tracks in zircon : an experimental study, , (1978), 1995.

Figures:

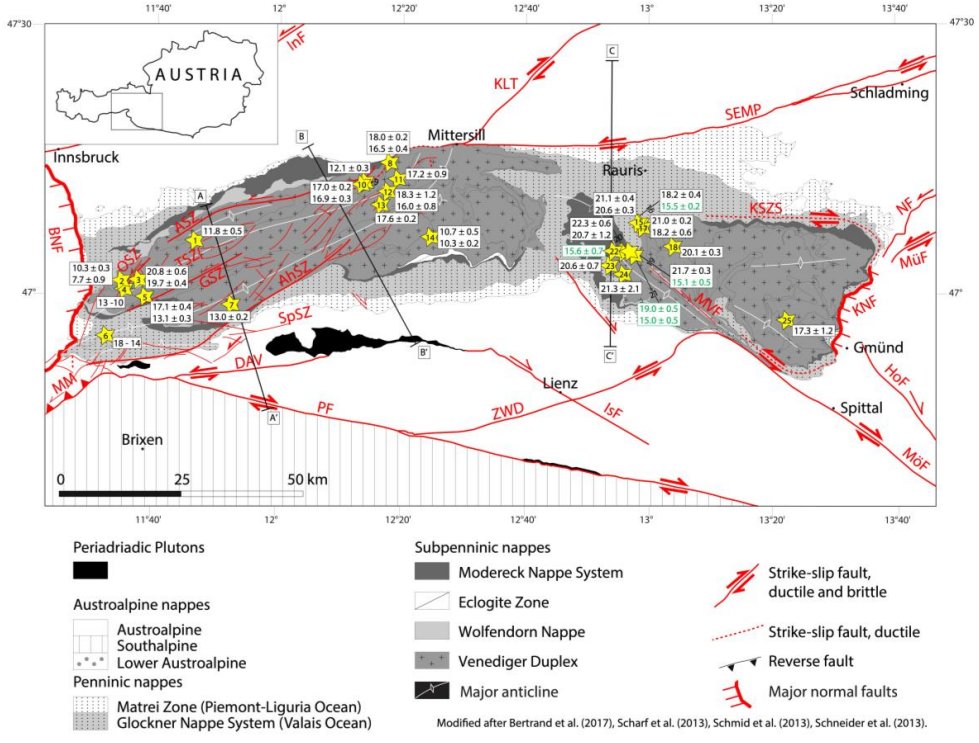

Fig. 1*: Tectonic map of the Tauern metamorphic dome modified after Bertrand et al. (2017), Schmid et al. (2013) and Schneider et al. (2013). Yellow stars on the map represent samples locations and numbers*

https://doi.org/10.5194/se-2019-162
Preprint. Discussion started: 30 October 2019

inside the stars refer to samples listed in Table 1. Range of weighted mean growth domain ages are indicated for each grain from this study and Gnos et al. (2015), labelled in black and green respectively on the map (see Table 5 for an exhaustive summary of all the ages). Only the spot date range is indicated for grains 4 and 6. Locations of AA', BB' and CC' cross sections are indicated by black lines and individual cross sections are presented in figure 6 together with monazite crystallization ages. Two normal faults delimit the western and eastern border of the TW, the Brenner Normal Fault (BNF) and the Katschberg Normal Fault (KNF) respectively. Note that the KNF prolongation results in dextral and sinistral strike-slips in the North and South respectively (KSZS: Katschberg Shear Zone System). Several sinistral strike-slip faults (AhSZ: Ahmtal Shear Zone; ASZ: Ahorn Shear Zone; DAV: Deferggen-Antholz-Vals Fault; GSZ: Greiner Shear Zone; InF: Inntal Fault; MüF: Mur-Müritz Fault; NF: Niedere Tauern Southern Fault; OSZ: Olperer Shear Zone; SEMP: Salzach-Ennstal-Mariazell-Puchberg Fault; SpSZ: Speikboden Shear Zone; TSZ: Tuxer Shear Zones; ZWD: Zwischenbergen-Wöllatratten and Drautal Faults), dextral shear zones (HoF: Hochstuhl Fault; IsF: Iseltal Fault; KLT: Königsee-Lammertal-Traunsee Fault; Mölltal Fault (MöF); Möll Valley Fault (MVF); PF: Pustertal Fault) and a reverse fault (MM: Meran-Maules Fault) are also visible in red on the map.

https://doi.org/10.5194/se-2019-162
Preprint. Discussion started: 30 October 2019

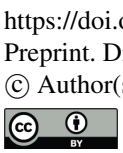

Solid Earth
Discussions
Open Access
EGU

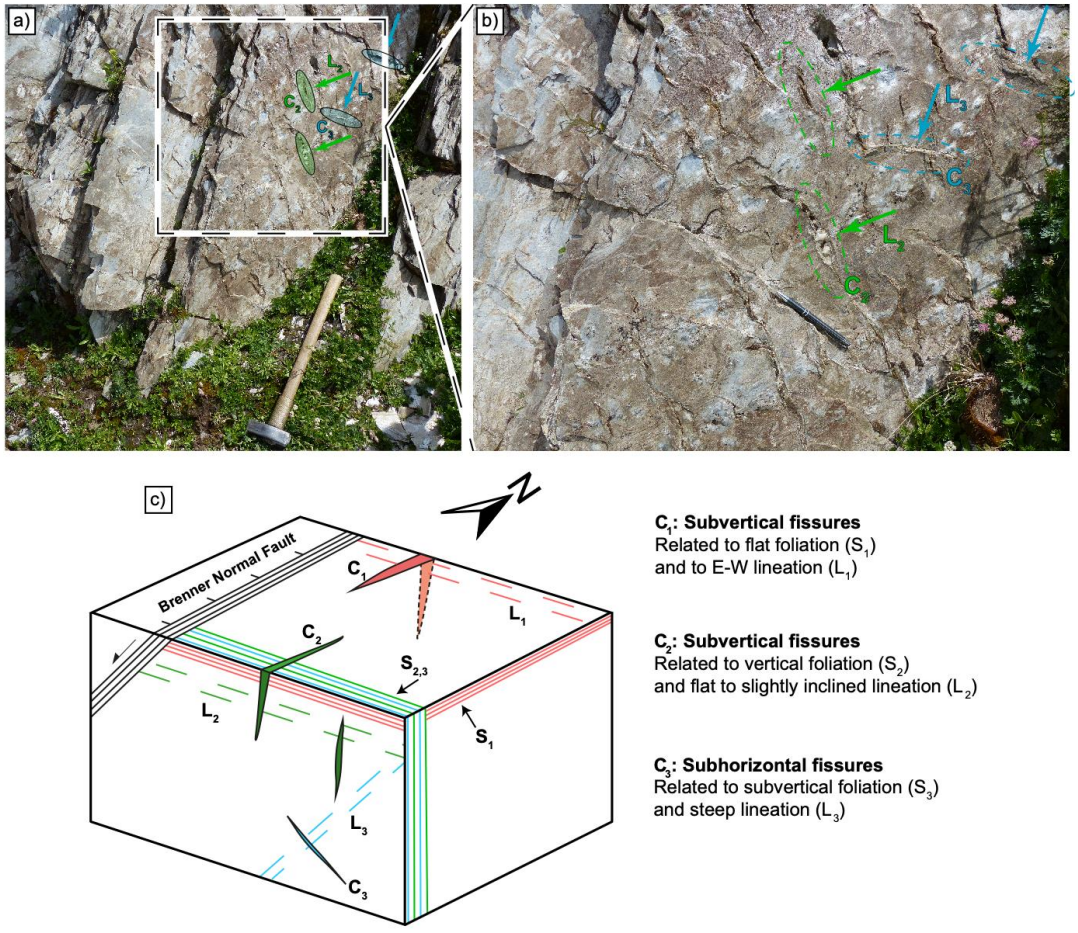

***Fig. 2**: a) Two generations of late fissures visible in an outcrop along the gravel road to Pfitscherjoch. Steeply oriented fissures (C_2: ~090/65) are older and deformed (green ellipses), and seem related to flat lineation (L_2: ~250/30, green arrows) visible on some of the foliation planes. Younger and flatter oriented fissures (C_3: ~085/30) are strait (blue ellipses), and seem related to a steeper lineation (L_3: 270/70, blue arrows). These observations indicate that a fissure can be deformed during its existence. Lengths of hammer handle is 60 cm. b) Enlargement of a). c) Schematic illustration of the 3 fissure generations observed in this study (C_1, C_2 and C_3), together with respective orientation, foliation (S_1, S_2 and S_3) and lineation (L_1, L_2 and L_3). The first fissure generation (C_1) is related to E-W extension, the second fissure generation (C_2) is linked to strike-slip movements and the third fissure generation (C_3) is related to the oblique-slip movements.*

https://doi.org/10.5194/se-2019-162
Preprint. Discussion started: 30 October 2019

Solid Earth
Discussions
Open Access
EGU

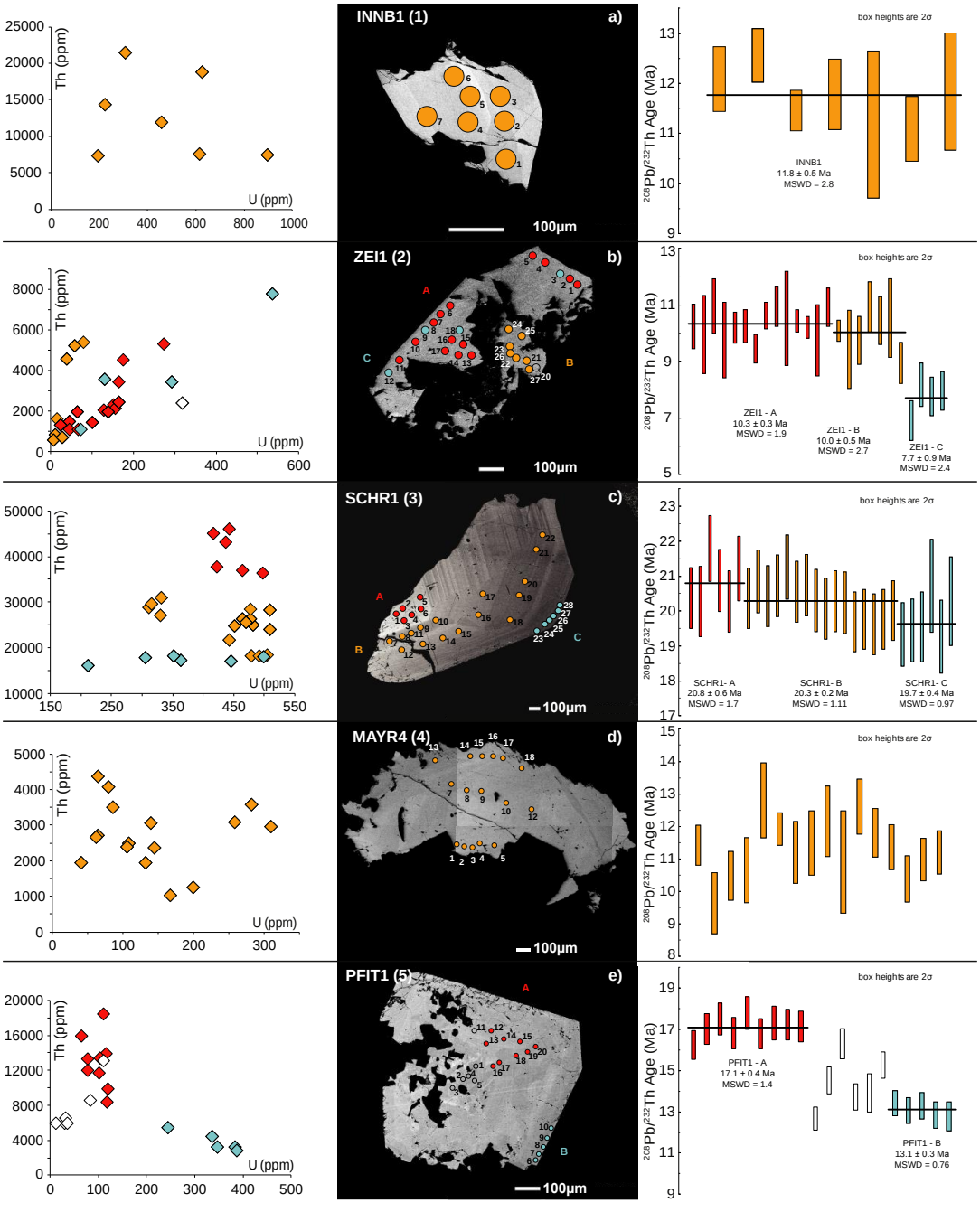

666

667

https://doi.org/10.5194/se-2019-162
Preprint. Discussion started: 30 October 2019

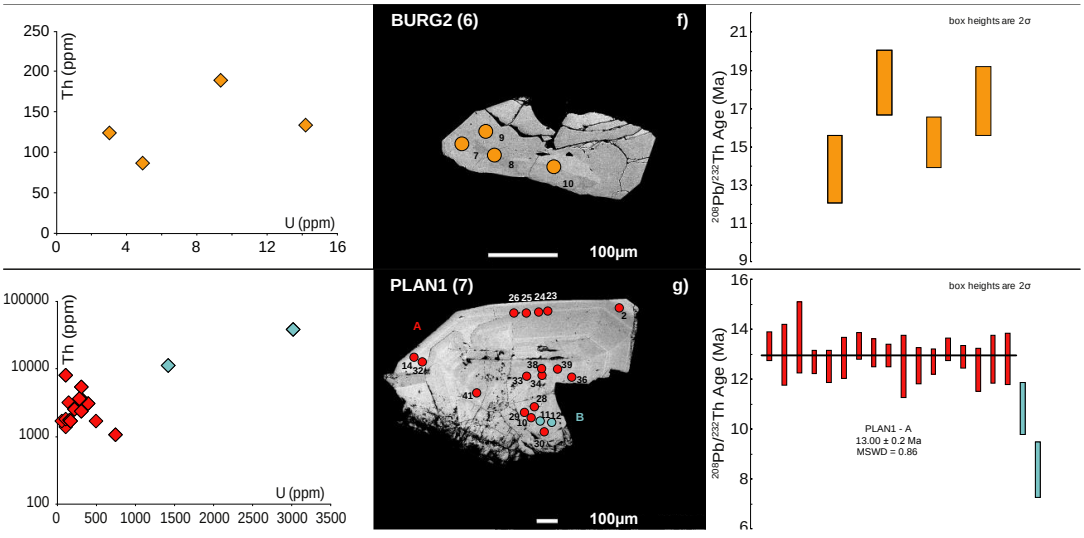

668

669 ***Fig. 3***: *Chemical, textural and geochronological information of monazite grains from the western TW. On*
670 *BSE images, colour-filled circles correspond to ion probe spot locations. Note that the square-shape*
671 *shading in grain 4 is due to an artefact of composing BSE images with diverse contrast.*

672

673

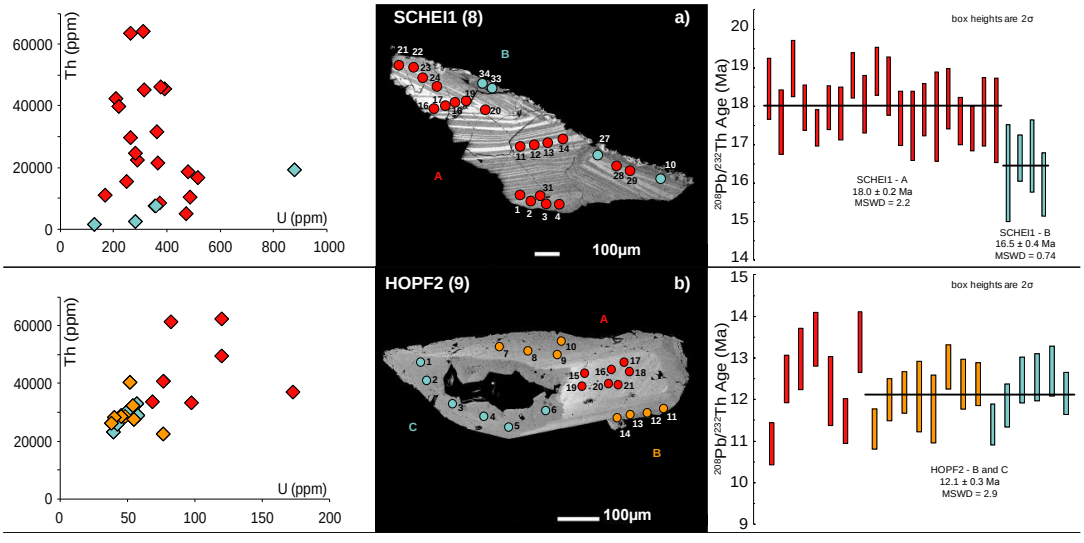

674

https://doi.org/10.5194/se-2019-162
Preprint. Discussion started: 30 October 2019

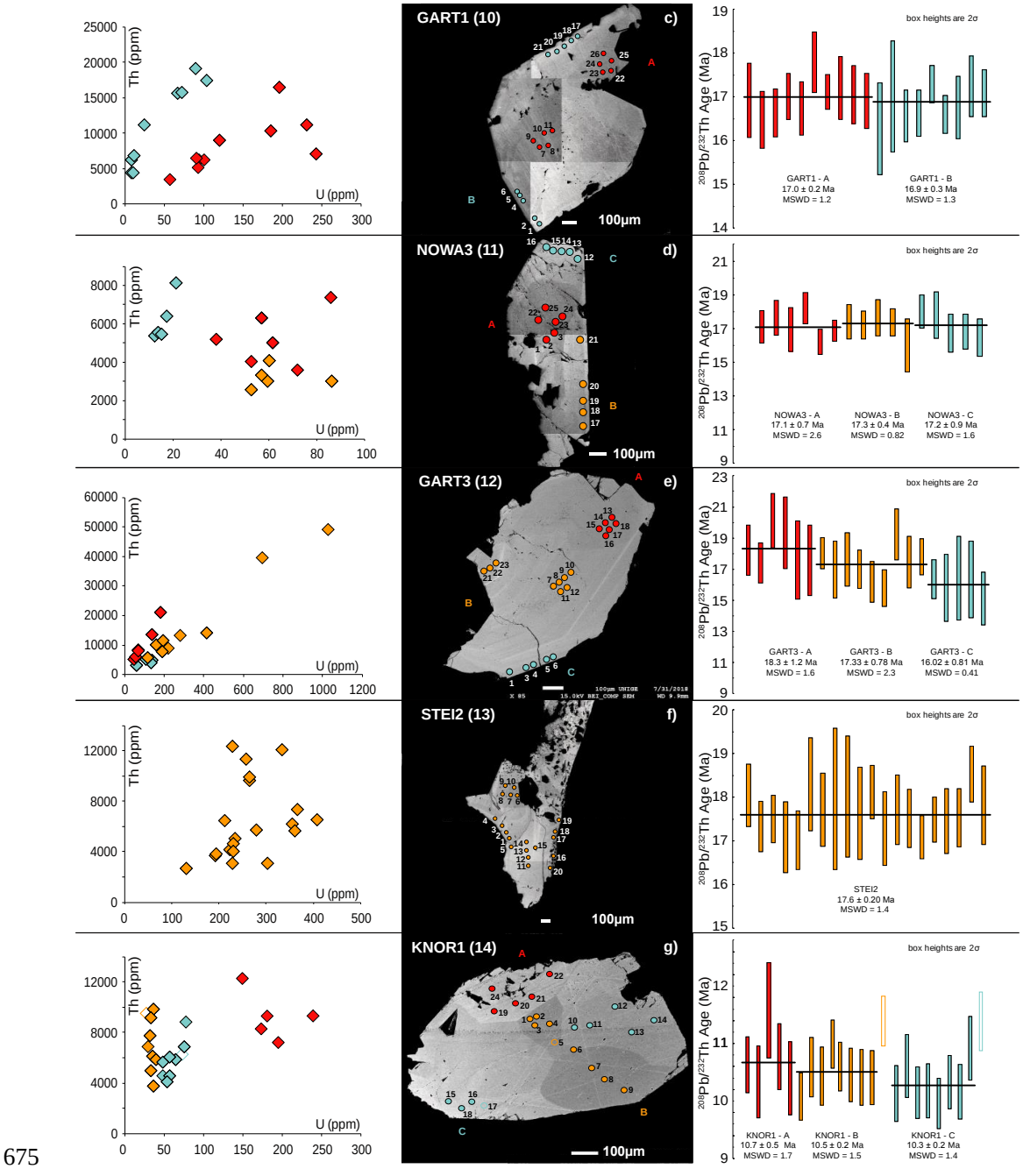

675

676 ***Fig. 4****: Chemical, textural and geochronological information of monazite grains from the central TW. On*
677 *BSE images, colour-filled circles correspond to ion probe spot locations. Note that the square-shape*
678 *shading in grains 10 and 11 is due to an artefact of composing BSE images with diverse contrast.*

https://doi.org/10.5194/se-2019-162
Preprint. Discussion started: 30 October 2019

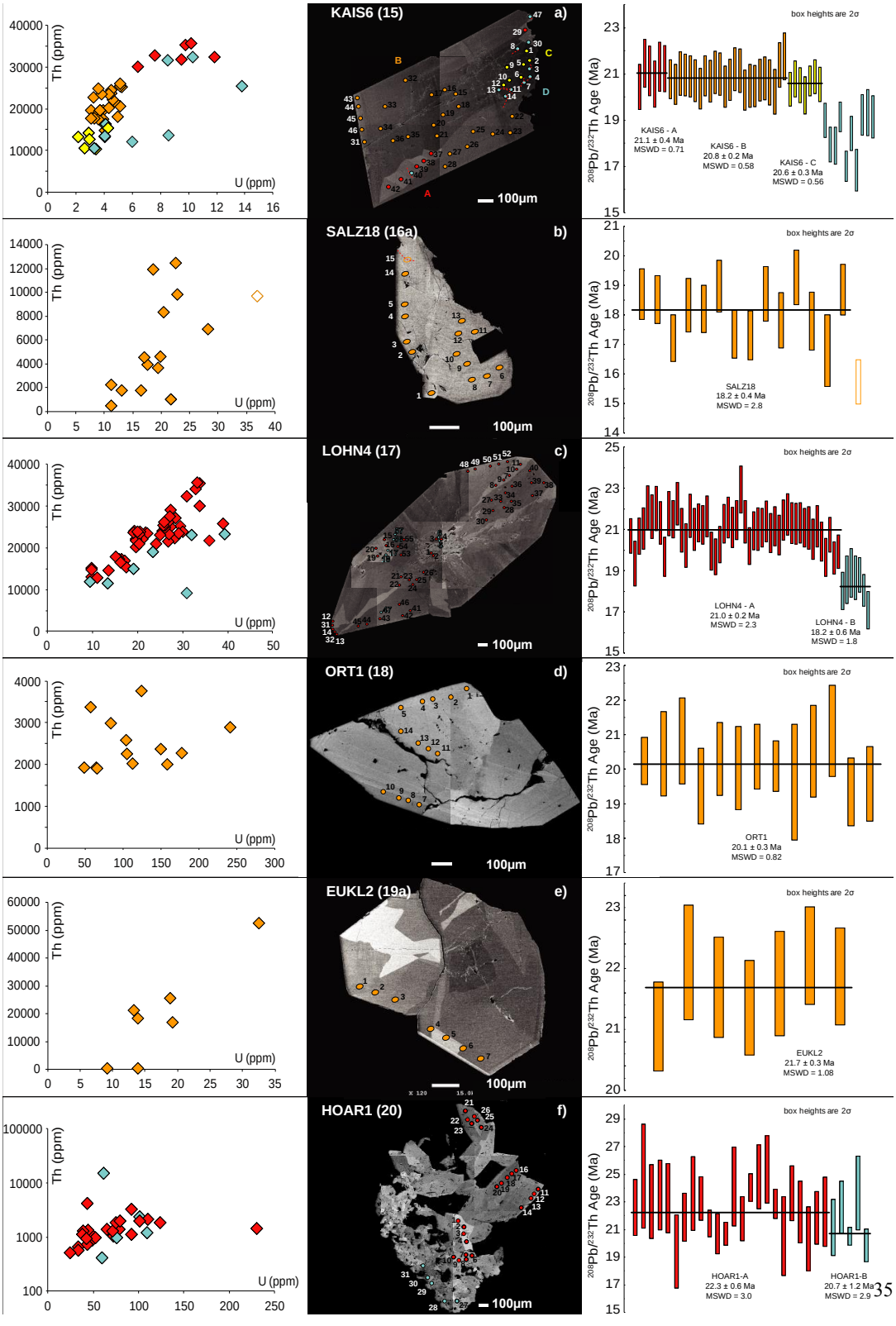

https://doi.org/10.5194/se-2019-162
Preprint. Discussion started: 30 October 2019

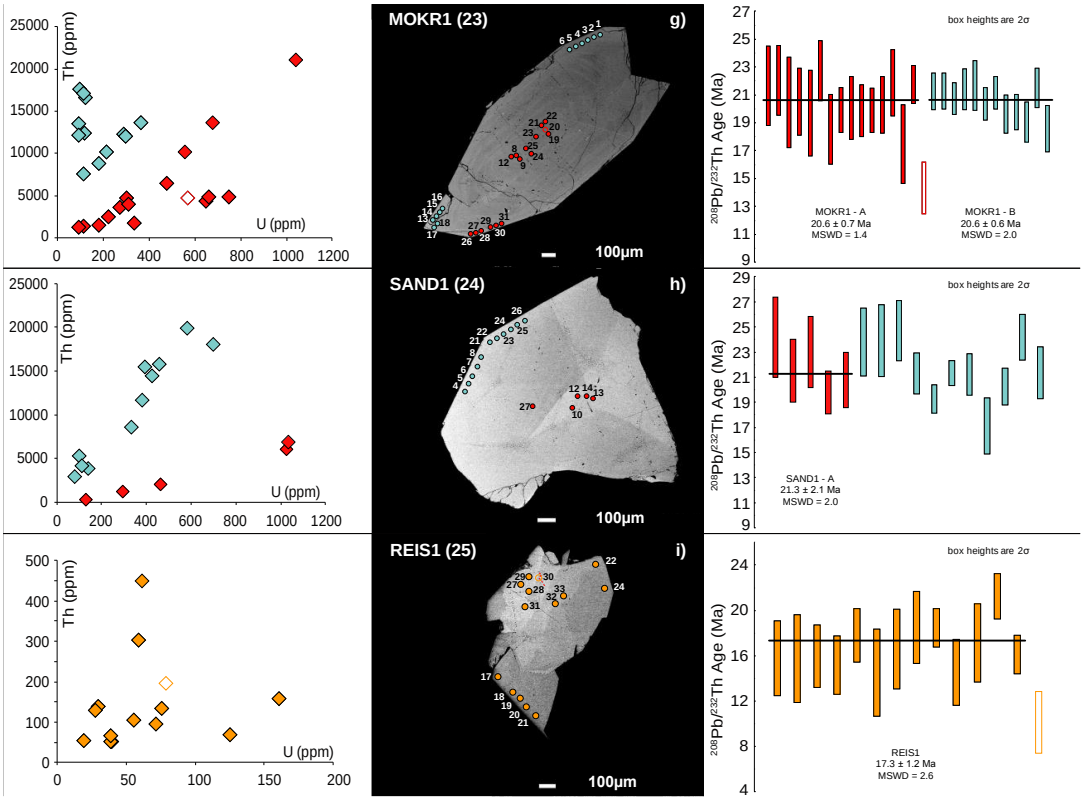

680

681 ***Fig. 5****: Chemical, textural and geochronological information of monazite grains from the eastern TW. On*
682 *BSE images, colour-filled circles correspond to ion probe spot locations. Note that the square-shape*
683 *shading in grains 15, 17, 18 and 20 is due to an artefact of composing BSE images with diverse contrast.*

684

https://doi.org/10.5194/se-2019-162
Preprint. Discussion started: 30 October 2019

Solid Earth
Discussions
Open Access
EGU

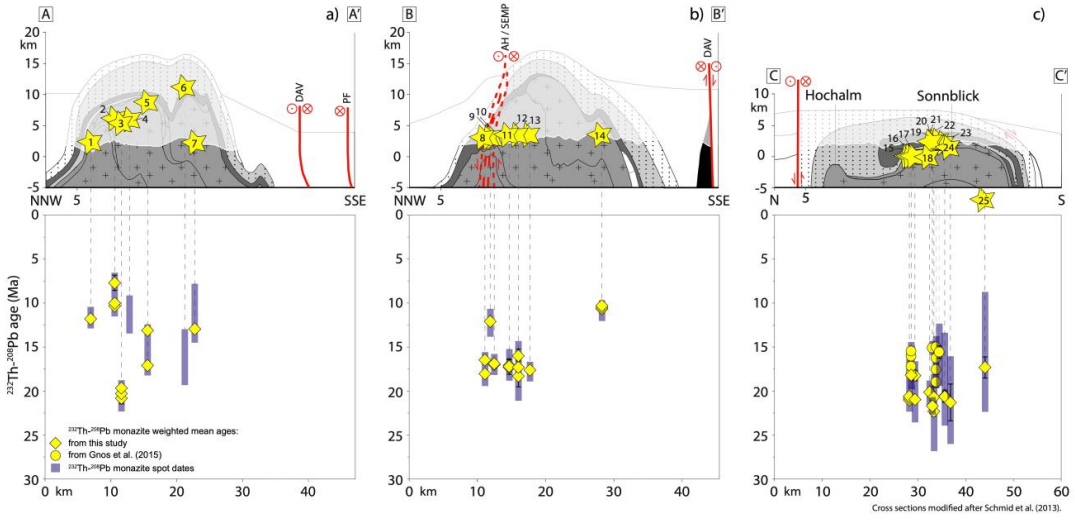

685

686 ***Fig. 6****: Cross sections of (a) the western, (b) the central part of the western subdome and (c) western end*
687 *of the eastern subdome, modified after Schmidt et al. (2013). See figure 1 for locations and legend. Sample*
688 *locations are indicated by yellow stars and identified by sample numbers listed in Table 1. Monazite*
689 *crystallization ages are present in the lower part of the figure and are linked to each sample by light-grey*
690 *dashed lines. Weighted mean ages from this study and from Gnos et al. (2015) are indicated by yellow*
691 *diamonds and yellow circles, respectively, and blue bars correspond to the range of single spot dates.*

692

https://doi.org/10.5194/se-2019-162
Preprint. Discussion started: 30 October 2019

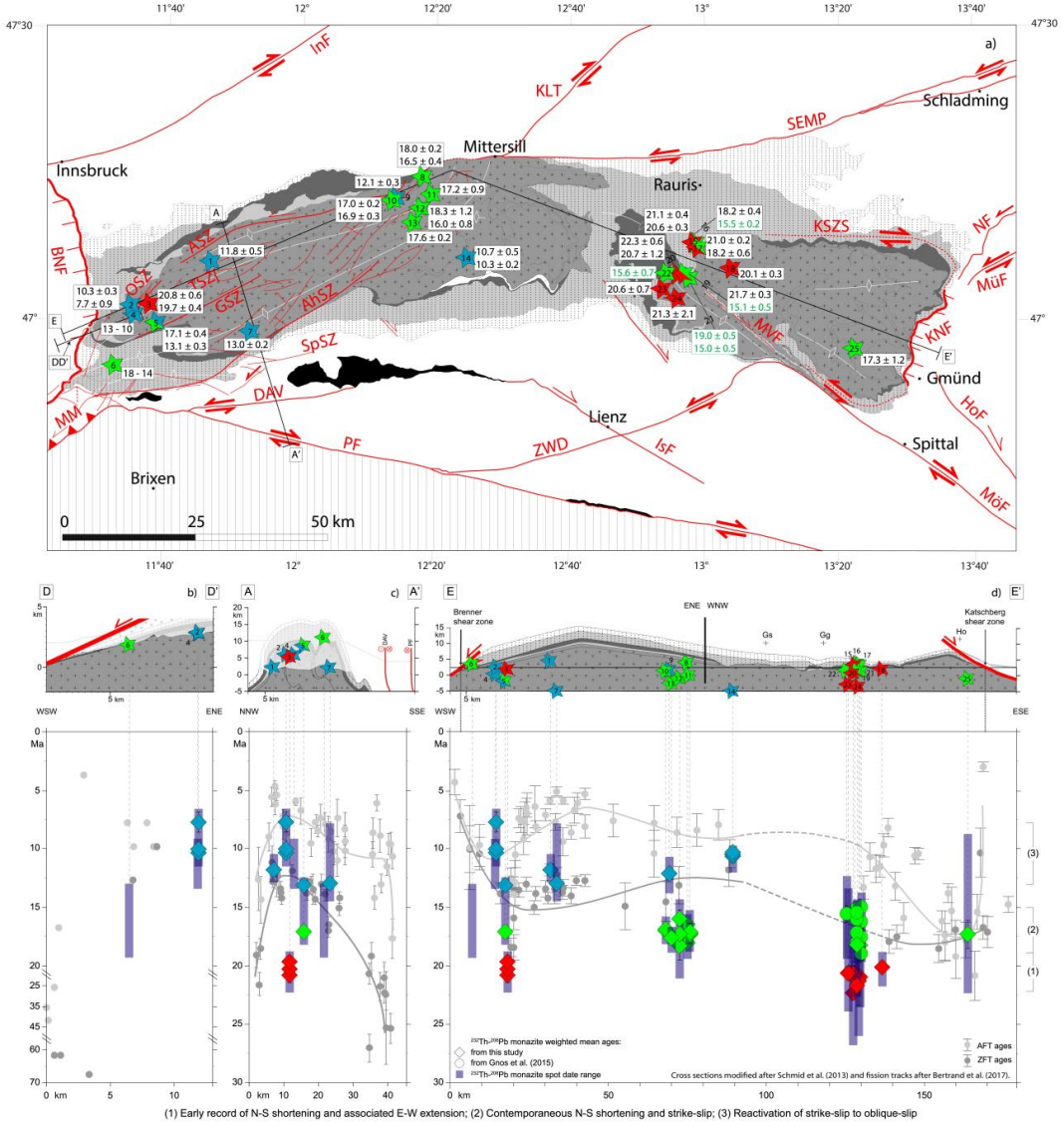

693

694 ***Fig. 7****: a) Map of the Tauern dome from figure 1 with samples location colored as function of deformation*
695 *episodes (colored stars). See figure 1 for legend. b) DD' NE-SW cross section perpendicular to the BNF, c)*
696 *AA' NW-SE cross section perpendicular to the axial plane of the western sub-dome and d) DD'*
697 *longitudinal cross section parallel to the main axial plane of the Tauern metamorphic dome, modified*
698 *after Bertrand et al. (2017). In the upper part, colored and numbered stars correspond to samples*
699 *locations and are linked to corresponding Th-Pb monazite ages by dashed vertical lines. Sample numbers*

https://doi.org/10.5194/se-2019-162
Preprint. Discussion started: 30 October 2019

700 *refer to Table 1. In the lower part, monazite weighted mean ages from this study and from Gnos et al.*
701 *(2015) are labelled by colored diamond and circles, respectively, and the range of single spot dates is*
702 *depicted by blue bars. The color code used for diamonds and circles follow deformation episodes*
703 *explained in the discussion. Note that most error bars are smaller than the size of the diamonds and*
704 *circles. Zircon and apatite fission tracks are from the Bertrand et al. (2017) compilation, light- and dark-*
705 *grey dots with error bars, are displayed for comparison. Square brackets shown to the right delimit the*
706 *main periods of monazite growth discussed in the text.*

707

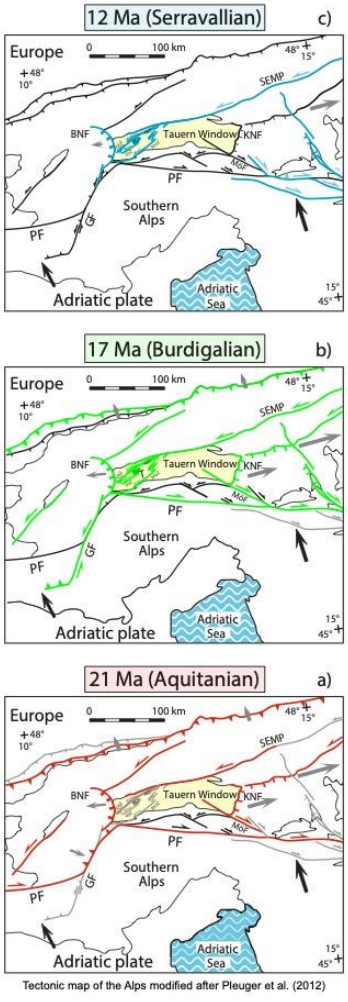

Tectonic map of the Alps modified after Pleuger et al. (2012)

Fig. 8*: Tectonic map of the Alps based on Pleuger et al. (2012) showing active Cenozoic faults at ca. 21 (in red), 17 (in green) and 12 Ma (in blue) respectively. Note that after 17 Ma the Giudicarie Fault (GF) becomes active and hence the Periadriatic Fault (PF) and the Mölltal Fault (MöF, dextral fault at the southeastern corner of the TW) become inactive. Sinistral strike-slip faulting starts at ca. 19 Ma and is affecting the western and central parts of the TW until at least 8 Ma. Future active faults are depicted in grey and inactive faults in black.*

https://doi.org/10.5194/se-2019-162
Preprint. Discussion started: 30 October 2019

722

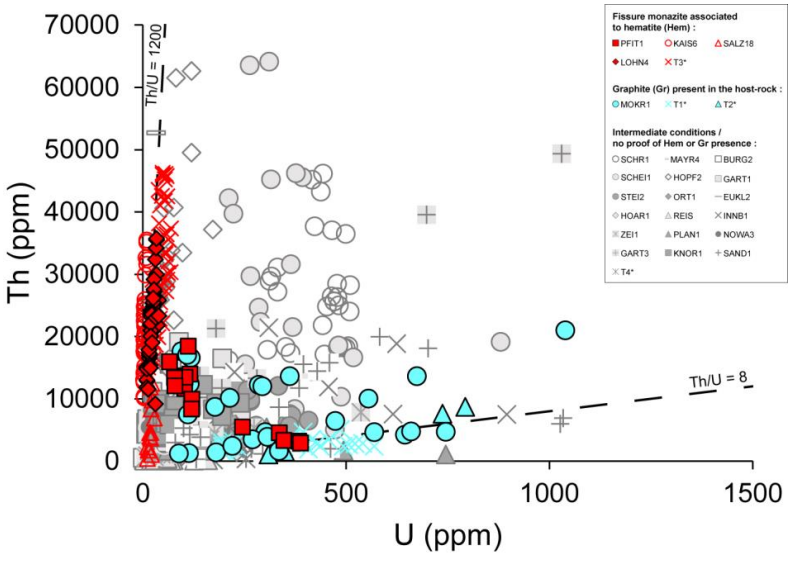

723

724 ***Fig. 9****: Th as function of U content obtained for all the monazite grains analysed in this study. Samples*
725 *indicated by an asterisk are from Gnos et al. (2015). Fissure monazite grains associated to hematite*
726 *(oxidizing conditions) are labelled in red whereas grains hosted in graphite bearing rocks (reducing*
727 *conditions) are labelled in blue. Samples with intermediate composition and/or for which we have no*
728 *information on the presence of hematite or graphite in the fissure environment are labelled in grey.*

729

https://doi.org/10.5194/se-2019-162
Preprint. Discussion started: 30 October 2019

Solid Earth Discussions

730 ***Tables:***

731 ***Table 1****: Summary of monazite samples investigated in this study and from Gnos et al. (2015). Samples*
732 *name, number, location, host-rock lithology, metamorphic degree and fissure mineral association are*
733 *provided. Samples with approximate finding location are marked with "approx.".*

Locality	Sample	N°	Latitude (°N)	Longitude (°E)	Remark	Host-rock	Host rock Alpine met.	Fissure mineral association	Reference	Ion probe
Western Tauern Window										
Innerböden, Zillertal, Tirol, Austria	INNB1	**1**	47°05.850'	011°47.667'	approx.	gneiss	AM	Qtz, Adl, Chl	this study	SwissSIMS
Zeischalm, Valsertal, Tirol, Austria	ZEI1	**2**	47°01.400'	011°35.767'	approx.	gneiss	AM	Qtz, Adl, Chl	this study	SwissSIMS
Schrammacher, Zillertal, Tirol, Italy	SCHR1	**3**	47°01.47'	011°38.60'	approx.	gneiss	AM	Qtz, Chl, Adl, Rt, Snt	this study	NordSim
Kluppen, Pfitschtal, Südtirol, Italy	MAYR4	**4**	47°00.400'	011°36.217'	approx.	gneiss	AM	Qtz, Adl, Ant, Cc, Rt, Xnt	this study	SwissSIMS
Pfitscherjoch, Tirol, Austria	PFIT1	**5**	46°59.65'	011°39.60'		mica schist	AM	Qtz, Hm, Adl, Trm, Rt, Brk, Ant, Syn, Asc	this study	NordSim
§ Burgumalpe, Pfitschtal, Südtirol, Italy	BURG2	**6**	46°55.217'	011°33.350'	approx.	serpentinite	GAT	Ilm, Rt, Cc	this study	SwissSIMS
Schwarzenbach, Ahrntal, Südtirol, Italy	PLAN1	**7**	46°58.641'	011°53.302'	approx.	gneiss	AM	Qtz, Adl	this study	SwissSIMS
Central Tauern Window										
Scheissgraben (Kotriesen), Habachtal, Salzburg, Austria	SCHEI1	**8**	47°14.483'	012°18.667'		mica schist	UGS	Qtz, Ab, Ant, Ank, Rt	this study	SwissSIMS
Hopffeldboden, Oberzulzbachtal, Salzburg, Austria	HOPF2	**9**	47°12.278'	012°14.844'		gneiss	GAT	Qtz, Ilm, Rt, Ant, Brk, Asc, Syn, Ap, Chl, Lm	this study	NordSim
Hopffeldgraben, Oberzulzbachtal, Salzburg, Austria	GART1	**10**	47°12.100'	012°14.167'		gneiss	GAT	Qtz, Adl, Ant, Rtl, Asc + Bt and Chl from EDS analyses	this study	SwissSIMS
Wildenkarer-Wald, Habachtal, Salzburg, Austria	NOWA3	**11**	47°12.633'	012°20.000'	approx.	gneiss	GAT	Qtz, Ab, Adl	this study	SwissSIMS
Beryller, Untersulzbachtal, Salzburg, Austria	GART3	**12**	47°11.250'	012°18.517'	approx.	gneiss	AM	Qtz, Adl	this study	SwissSIMS
Sattelkar, Obersulzbachtal, Salzburg, Austria	STEI2	**13**	47°09.783'	012°17.250'	approx.	gneiss	AM	Qtz, Adl, Rt, Chl	this study	SwissSIMS
Innerer Knorrkogel, Osttirol, Austria	KNOR1	**14**	47°06.117'	012°25.183'		gneiss	AM	Adl, Qtz, Chl	this study	NordSim
Eastern Tauern Window										
* Kaiserer Steinbruch,Hüttwinkeltal, Rauris, Salzburg, Austria	KAIS6	**15**	47°07.787'	012°58.708'		meta-arenite	GAT	Qtz, Adl, Trm, Cc, Hm, Rt, Chl	this study	NordSim
* Lohninger Quarry, Hüttwinkeltal, Rauris, Salzburg, Austria	SALZ18	**16a**	47°07.20'	012°59.33'		meta-arenite	GAT	Qtz, Adl, Trm, Cc, Hm, Rt, Chl	this study	NordSim
** Lohninger Quarry, Hüttwinkeltal, Rauris, Salzburg, Austria*	*T3*	***16b***	*47°07.20'*	*012°59.33'*		*meta-arenite*	*GAT*	*Alb, Qtz, Trm, Hm, Rt*	*Gnos et al., 2015*	*NordSim*
* Lohninger Quarry, Hüttwinkeltal, Rauris, Salzburg, Austria	LOHN4	**17**	47°07.20'	012°59.33'		meta-arenite	GAT	Qtz, Adl, Trm, Cc, Hm, Rt, Chl	this study	NordSim
Ortberg bei Böckstein, Salzburg, Austria	ORT1	**18**	47°05.150'	013°04.217'		granitic gneiss	GAT	Qtz, Adl, Rt, Chl, Ap	this study	SwissSIMS
Euklaskluft, Griesswies, Salzburg, Austria	EUKL2	**19a**	47°04.683'	012°57.250'		Bt-Mu schist	GAT	Alb, Pyr, Qtz, Rt, Chl, euclase, Xnt, goethite-todorokite-nordstrandite	this study	NordSim
Euklaskluft, Griesswies, Salzburg, Austria	*T2*	***19b***	*47°04.683'*	*012°57.250'*		*Bt-Mu schist*	*GAT*	*Alb, Pyr, Qtz, Rt, Chl, euclase, Xnt, goethite-todorokite-nordstrandite*	*Gnos et al., 2015*	*NordSim*
Hocharn, Kärnten, Austria	HOAR1	**20**	47°04.500'	012°56.083'		granitic gneiss	GAT	Qtz, Ab, Rt	this study	SwissSIMS
Erfurter Steig, Rauris, Salzburg	*T1*	***21***	*47°04.133'*	*012°57.917'*		*Bt-Mu schist*	*GAT*	*Qtz, Ab, Adl, phenakite, Rt, Cc*	*Gnos et al., 2015*	*NordSim*
Gjaidtroghöhe, Grosses Fleisstal, Kärnten	*T4*	***22***	*47°03.783'*	*012°54.650'*		*gneiss*	*GAT*	*Qtz, Ab, Ant/Rt,Chl, Cc*	*Gnos et al., 2015*	*NordSim*
Mokritzen, Kleines Fleisstal, Kärnten, Austria	MOKR1	**23**	47°03.033'	012°53.983'		aphite bearing schi	GAT	Qtz, Sid	this study	SwissSIMS
Sandkopf, Grosses Zirknitztal, Kärnten, Austria	SAND1	**24**	47°01.983'	012°56.05		banded gneiss	GAT	Qtz, Adl, Chl, Sid, Ant	this study	SwissSIMS
Kleiner Reisseck, Reisseckgruppe, Kärnten, Austria	REIS1	**25**	46°56.950'	013°22.433'		banded gneiss	AM	Qtz, Ant, Ab, Chl	this study	SwissSIMS

Ab = albite; Adl =adularia; Ank = ankerite; Ant = anatase; Ap = fluorapatite; Asc = Aeschynite; Brk = brookite; Cc =calcite; Chl =chlorite; Clc =clinochlore; Hm = hematite; Ilm = ilmenite; Lm =limonite; Pyr = pyrite; Qtz = quartz; Rt = rutile; Sd = Siderite; Snt = senaite; Str = strontianite; Syn = synchisite; Trm = tourmaline; Xnt = xenotime; Alpine metamorphism: AM (Amphibolite facies), GAT (Greenschist-amphibolite transition), UGS (Upper greenschist facies). Bloc in glacial

748

https://doi.org/10.5194/se-2019-162
Preprint. Discussion started: 30 October 2019

749 ***Table 2**: Summary of deformation phases in the Tauern metamorphic dome.*

Age [Ma]	Phase	Fault	Domain	Characteristics	Ref.	Remarks
Deformation phases						
~ 65	**D1**		Penninic nappes	Accretion and subduction of Piemont-Liguria Ocean	E	
~ 41	**D2**		Penninic and Subpenninic nappes	Subduction of Valais Ocean and parts of the distal European margin	E	
~ 35	**D3**		Central TW	Exhumation of high-pressure units	E	Folding of D2 thrust, decompression
~ 29	**D4**		Subpenninic nappes	European slab break off, Venediger Duplex formation and Tauern ''Kristallisation''	E	Contemporaneous intrusion of Periadriatic plutons and incipient
23 - 21			East of the Giudicarie Belt	Incipient indentation of the Southalpine Units in the Eastern Alps	D, E	
~ 17	**D5**		TW	Indentation, doming and lateral extrusion	E	
Faults motion						
33 - 15		ASZ	Western TW	Sinistral ductile shear	F, G	Ductile continuation of the SEMP fault
24 - 12		TSZ	Western TW	Sinistral ductile shear	B, F	
28 - 7		GSZ	Western TW	Sinistral ductile shear	F	
21 - 10		BNF	Western TW	Normal fault	C	
22 - 13		KNF	Eastern TW	Normal fault	C	

A: Bertrand et al., 2017, 2015; B: Blackenburg et al., 1989; C: Favaro et al., 2017; D: Scharf et al. 2013; E: Schmid et al., 2013; F: Schneider et al., 2013; G: Rosenberg and Schneider, 2008. ASZ: Ahorn Shear Zone, BNF: Brenner Normal Fault, GSZ: Greiner Shear Zone, KNF: Katschberg
750 Normal Fault, SEMP: Salzach-Ennstal-Mariazell-Puchberg fault, TSZ: Tuxer Shear Zones.

751

752 ***Table 3**: Th-U-Pb analyses of monazite by ion microprobe (SwissSIMS). Analyses resulting in unreliable*
753 *dates (e.g. presence of cracks, affected by Pbc causing high uncertainty) were not considered and are*
754 *written in italic.*

Groups	Analysis ID	U (ppm)	Th (ppm)	Th/U	$^{204}Pb/^{206}Pb$	1σ (%)	$^{208}Pb/^{206}Pb$	1σ (%)	f208 (%)	207 - corr $^{208}Pb/^{232}Th$	207 - corr 1σ (%)	207-corr spot ages $^{208}Pb/^{232}Th$ Age (Ma)	207-corr spot ages 1σ (abs.)
Western Tauern Window													
	INNB1@01	196	7265	37	0.0309	13	6.5	4.4	18	0.000599	2.7	12.10	0.32
	INNB1@02	310	21420	69	0.0221	14	14.9	2.6	6	0.000622	2.1	12.57	0.27
	INNB1@03	225	14273	63	0.0208	16	12.9	2.8	6	0.000568	1.8	11.47	0.20
	INNB1@04	896	7479	8	0.0097	15	2.5	1.2	15	0.000584	3.0	11.80	0.35
	INNB1@05	457	11912	26	0.0117	15	6.9	2.4	7	0.000554	6.6	11.19	0.73

https://doi.org/10.5194/se-2019-162
Preprint. Discussion started: 30 October 2019

	INNB1@06	625	18830	30	0.0145	12	7.0	1.0	8	0.000550	2.9	11.11	0.33
	INNB1@07	616	7547	12	0.0110	15	3.2	2.5	13	0.000587	4.9	11.85	0.59
	INNB1@8	*1017*	*14593*	*14*	*0.0100*	*19*	*3.8*	*4.0*	*10*	*0.000605*	*13.1*	*12.23*	*1.61*
A	**ZEI1@01**	45	1507	33	0.0185	21	7.2	2.2	6	0.000508	3.9	10.27	0.40
	ZEI1@02	64	1959	31	0.0177	24	6.7	2.5	5	0.000494	7.0	9.99	0.70
	ZEI1@04	45	1127	25	0.0156	25	6.3	2.4	6	0.000545	4.4	11.00	0.49
	ZEI1@05	24	1315	55	0.0212	26	9.3	2.8	6	0.000485	6.9	9.79	0.68
	ZEI1@06	100	1462	15	0.0150	18	3.9	1.6	9	0.000506	2.7	10.23	0.28
	ZEI1@07	155	2166	14	0.0078	24	4.3	1.6	7	0.000509	2.8	10.28	0.29
	ZEI1@08	164	2436	15	0.0112	21	3.5	1.7	9	0.000469	2.7	9.47	0.25
	ZEI1@10	139	1998	14	0.0083	21	3.9	1.4	6	0.000528	2.2	10.66	0.23
	ZEI1@11	66	1105	17	0.0134	20	4.0	2.7	8	0.000544	3.3	10.99	0.36
	ZEI1@13	176	4526	26	0.0114	16	6.6	2.9	4	0.000523	8.0	10.56	0.85
	ZEI1@14	165	3466	21	0.0098	19	5.4	1.3	5	0.000518	1.9	10.47	0.20
	ZEI1@15	274	5341	20	0.0107	21	5.4	1.3	8	0.000507	1.9	10.24	0.19
	ZEI1@16	152	2326	15	0.0091	19	4.2	1.3	7	0.000484	6.5	9.77	0.63
	ZEI1@17	128	2068	16	0.0157	15	4.6	1.4	10	0.000542	3.1	10.96	0.34
B	**ZEI1@21**	79	5428	69	0.0229	17	13.9	2.6	3	0.000501	1.9	10.13	0.19
	ZEI1@22	38	4567	121	0.0274	16	22.5	4.9	3	0.000468	7.4	9.46	0.70
	ZEI1@23	57	5243	92	0.0247	20	18.4	2.1	4	0.000484	4.3	9.78	0.42
	ZEI1@24	12	862	73	0.0262	21	16.3	2.5	3	0.000543	4.1	10.97	0.45
	ZEI1@25	*7*	594	79	0.0245	22	16.2	2.6	3	0.000519	4.1	10.49	0.43
	ZEI1@26	16	1649	103	0.0342	19	20.8	2.7	3	0.000523	6.6	10.57	0.70
	ZEI1@27	29	734	26	0.0102	22	5.7	2.1	3	0.000444	4.1	8.96	0.36
C	**ZEI1@03**	129	3579	28	0.0097	41	6.4	3.2	5	0.000342	5.1	6.92	0.35
	ZEI1@09	536	7817	15	0.0063	35	4.0	3.1	5	0.000405	4.7	8.19	0.39
	ZEI1@12	73	1115	15	0.0104	24	3.2	2.8	7	0.000384	4.4	7.77	0.34
	ZEI1@18	292	3456	12	0.0072	26	3.1	3.7	7	0.000394	4.3	7.97	0.34
	ZEI1@19	*201*	*516*	*3*	*0.0055*	*22*	*1.0*	*1.6*	*16*	*0.000674*	*4.4*	*13.61*	*0.59*
	ZEI1@20	*319*	*2418*	*8*	*0.0044*	*27*	*2.1*	*1.5*	*5*	*0.000542*	*2.9*	*10.95*	*0.32*
	MAYR4@01	145	2356	16	0.0095	19	4.9	1.7	4	0.000566	2.7	11.43	0.31
	MAYR4@02	259	3071	12	0.0092	20	3.1	4.0	6	0.000477	5.0	9.64	0.48
	MAYR4@03	282	3585	13	0.0101	21	3.4	2.0	5	0.000519	3.6	10.49	0.37
	MAYR4@04	310	2961	10	0.0075	22	3.1	2.2	5	0.000527	4.7	10.66	0.50
	MAYR4@05	200	1254	6	0.0085	18	2.1	2.2	10	0.000635	4.5	12.84	0.58
	MAYR4@07	65	2712	42	0.0241	15	9.9	1.8	7	0.000591	2.1	11.95	0.25
	MAYR4@08	109	2480	23	0.0161	17	6.1	1.8	7	0.000555	4.3	11.21	0.48
	MAYR4@09	139	3060	22	0.0182	15	5.5	1.8	9	0.000569	4.3	11.50	0.50
	MAYR4@10	132	1950	15	0.0099	20	4.6	1.8	5	0.000603	4.5	12.19	0.55

https://doi.org/10.5194/se-2019-162
Preprint. Discussion started: 30 October 2019

	MAYR4@12	167	1038	6	0.0088	19	2.0	2.3	8	0.000541	7.3	10.92	0.79
	MAYR4@13	41	1945	47	0.0264	18	11.0	2.3	7	0.000626	3.4	12.64	0.43
	MAYR4@14	63	2657	42	0.0252	17	10.1	2.0	6	0.000585	3.2	11.82	0.38
	MAYR4@15	65	4371	67	0.0263	19	12.4	3.4	5	0.000563	3.1	11.38	0.35
	MAYR4@16	80	4071	51	0.0220	18	11.7	1.9	4	0.000514	3.4	10.39	0.36
	MAYR4@17	86	3506	41	0.0245	16	9.9	1.9	6	0.000544	3.0	10.99	0.33
	MAYR4@18	106	2400	23	0.0149	18	5.9	2.5	7	0.000555	3.0	11.21	0.34
	MAYR4@06	*253.4*	*583*	*2*	*0.0049*	*22*	*0.9*	*2.9*	*14*	*0.000630*	*7.9*	*12.74*	*1.01*
	MAYR4@11	*220.7*	*876*	*4*	*0.0042*	*26*	*1.3*	*5.1*	*11*	*0.000507*	*10.1*	*10.24*	*1.03*
	BURG2@07	5	87	18	0.0177	21	3.4	3.1	9	0.000686	6.4	13.86	0.89
	BURG2@08	3	123	41	0.0246	18	6.0	2.7	11	0.000911	4.6	18.41	0.85
	BURG2@09	14	133	9	0.0086	25	2.3	2.9	4	0.000755	4.4	15.26	0.67
	BURG2@10	9	188	20	0.0165	20	5.2	3.9	6	0.000863	5.2	17.44	0.90
	BURG2@11	*0.3*	*522*	*1789*	*0.1703*	*27*	*26.6*	*12.2*	*8*	*0.000691*	*10.5*	*13.96*	*1.47*
	BURG2@12	*0.7*	*7*	*9*	*0.0311*	*19*	*2.1*	*4.4*	*43*	*0.001205*	*14.5*	*24.33*	*3.54*
	BURG2@13	*169.2*	*1492*	*9*	*0.0045*	*58*	*1.7*	*5.5*	*8*	*0.000455*	*16.5*	*9.18*	*1.51*
A	**PLAN1@02**	113	7948	71	0.0216	17	9.8	3.3	9	0.000662	2.1	13.38	0.29
	PLAN1@10	391	3061	8	0.0109	17	2.3	1.4	18	0.000644	4.7	13.02	0.61
	PLAN1@14	304	2341	8	0.0084	22	2.2	1.5	15	0.000680	5.2	13.74	0.72
	PLAN1@23	226	2607	12	0.0044	19	3.4	1.5	4	0.000631	1.9	12.74	0.24
	PLAN1@24	220	2507	11	0.0049	19	3.3	1.0	3	0.000622	2.6	12.56	0.33
	PLAN1@25	160	1770	11	0.0053	19	3.2	1.0	6	0.000638	3.2	12.89	0.42
	PLAN1@26	169	1669	10	0.0071	16	2.9	1.0	6	0.000662	2.0	13.38	0.27
	PLAN1@28	296	3609	12	0.0066	13	3.6	0.8	6	0.000649	2.2	13.11	0.29
	PLAN1@29	305	5434	18	0.0067	13	5.1	0.7	4	0.000643	1.8	13.00	0.23
	PLAN1@30	290	3623	12	0.0081	14	3.7	0.9	5	0.000621	5.0	12.54	0.63
	PLAN1@32	745	1074	1	0.0021	19	0.5	1.1	11	0.000623	2.9	12.58	0.36
	PLAN1@33	494	1711	3	0.0030	16	1.1	5.9	9	0.000631	2.0	12.75	0.26
	PLAN1@34	324	3459	11	0.0060	13	3.1	0.8	7	0.000656	1.7	13.25	0.23
	PLAN1@36	148	3174	21	0.0105	15	5.4	1.0	6	0.000640	1.7	12.94	0.23
	PLAN1@38	107	1401	13	0.0068	16	3.7	1.3	5	0.000614	3.5	12.41	0.44
	PLAN1@39	61	1665	27	0.0136	15	7.0	1.4	5	0.000636	3.7	12.85	0.48
	PLAN1@41	103	1779	17	0.0128	12	4.7	1.3	7	0.000636	4.1	12.86	0.52
B	**PLAN1@11**	1429	11090	8	0.0109	23	2.4	2.2	18	0.000537	4.9	10.85	0.53
	PLAN1@12	3026	39046	13	0.0059	38	2.6	2.7	9	0.000415	6.7	8.39	0.56
	PLAN1@01	*146*	*1072*	*7*	*0.0281*	*13*	*2.3*	*3.1*	*48*	*0.000858*	*7.4*	*17.34*	*1.28*
	PLAN1@03	*94*	*983*	*10*	*0.0335*	*10*	*2.4*	*2.6*	*54*	*0.000807*	*8.5*	*16.31*	*1.38*
	PLAN1@04	*269*	*1909*	*7*	*0.0151*	*17*	*2.1*	*1.7*	*28*	*0.000623*	*10.2*	*12.59*	*1.28*

https://doi.org/10.5194/se-2019-162
Preprint. Discussion started: 30 October 2019

PLAN1@05	*253*	*836*	*3*	*0.0178*	*14*	*1.3*	*1.9*	*54*	*0.000825*	*11.1*	*16.66*	*1.85*
PLAN1@06	*328*	*1009*	*3*	*0.0191*	*15*	*1.6*	*4.2*	*46*	*0.001041*	*17.5*	*21.04*	*3.69*
PLAN1@07	*338*	*2232*	*7*	*0.0138*	*15*	*1.6*	*4.2*	*34*	*0.000444*	*19.2*	*8.98*	*1.72*
PLAN1@08	*179*	*1205*	*7*	*0.0143*	*20*	*2.2*	*1.9*	*25*	*0.000713*	*3.7*	*14.40*	*0.53*
PLAN1@09	*490*	*3382*	*7*	*0.0155*	*16*	*2.1*	*3.1*	*28*	*0.000694*	*6.2*	*14.03*	*0.87*
PLAN1@13	*656*	*638*	*1*	*0.0063*	*18*	*0.6*	*4.0*	*42*	*0.000861*	*11.8*	*17.40*	*2.05*
PLAN1@15	*291*	*2207*	*8*	*0.0185*	*14*	*2.3*	*2.7*	*32*	*0.000744*	*6.2*	*15.03*	*0.92*
PLAN1@16	*297*	*1902*	*6*	*0.0181*	*14*	*2.1*	*2.7*	*33*	*0.000738*	*12.5*	*14.91*	*1.86*
PLAN1@17	*274*	*2190*	*8*	*0.0131*	*19*	*2.2*	*2.3*	*23*	*0.000744*	*8.3*	*15.03*	*1.25*
PLAN1@18	*203*	*1676*	*8*	*0.0101*	*21*	*2.5*	*2.4*	*15*	*0.000807*	*8.9*	*16.31*	*1.44*
PLAN1@19	*250*	*7810*	*31*	*0.0249*	*12*	*6.3*	*4.2*	*15*	*0.000739*	*4.6*	*14.94*	*0.68*
PLAN1@20	*280*	*4174*	*15*	*0.0170*	*13*	*3.8*	*2.0*	*17*	*0.000693*	*5.3*	*14.00*	*0.75*
PLAN1@21	*220*	*1725*	*8*	*0.0205*	*11*	*2.6*	*2.6*	*31*	*0.000685*	*14.5*	*13.85*	*2.00*
PLAN1@22	*467*	*751*	*2*	*0.0144*	*13*	*1.0*	*12.0*	*57*	*0.001003*	*37.1*	*20.26*	*7.52*
PLAN1@27	*262*	*1257*	*5*	*0.0035*	*19*	*1.9*	*3.9*	*7*	*0.000574*	*9.3*	*11.59*	*1.07*
PLAN1@31	*437*	*432*	*1*	*0.0035*	*14*	*0.4*	*2.4*	*25*	*0.000733*	*6.8*	*14.80*	*1.00*
PLAN1@35	*242*	*3561*	*15*	*0.0162*	*13*	*3.7*	*2.5*	*18*	*0.000747*	*4.6*	*15.08*	*0.70*
PLAN1@37	*116*	*460*	*4*	*0.0034*	*21*	*1.1*	*2.1*	*9*	*0.000498*	*9.1*	*10.07*	*0.91*
PLAN1@40	*73*	*421*	*6*	*0.0055*	*22*	*1.7*	*2.3*	*15*	*0.000568*	*9.2*	*11.47*	*1.06*

Central Tauern Window

A	**SCHEI1@01**	487	10337	21	0.0145	11	5.6	0.9	10	0.000914	2.2	18.47	0.40
	SCHEI1@02	364	31582	87	0.0169	15	15.3	3.4	4	0.000872	2.4	17.61	0.42
	SCHEI1@03	369	21511	58	0.0180	12	10.5	4.1	7	0.000941	2.0	19.01	0.37
	SCHEI1@04	481	18572	39	0.0173	14	8.2	3.7	8	0.000890	1.7	17.99	0.30
	SCHEI1@11	315	45235	143	0.0230	15	23.6	4.3	4	0.000864	1.4	17.46	0.24
	SCHEI1@12	393	45593	116	0.0184	11	21.4	3.7	3	0.000890	1.6	17.99	0.29
	SCHEI1@13	377	46191	123	0.0326	9	23.6	2.9	5	0.000882	1.9	17.83	0.35
	SCHEI1@14	211	42211	200	0.0293	9	24.9	3.9	5	0.000932	1.6	18.83	0.30
	SCHEI1@16	265	29683	112	0.0196	7	26.0	2.5	1	0.000895	2.1	18.08	0.38
	SCHEI1@17	311	64103	206	0.0232	8	38.9	0.7	1	0.000937	1.7	18.94	0.31
	SCHEI1@18	263	63534	241	0.0260	7	41.4	0.7	1	0.000918	2.1	18.55	0.38
	SCHEI1@19	518	16629	32	0.0071	12	9.1	0.7	1	0.000877	2.0	17.71	0.35
	SCHEI1@20	223	39711	178	0.0225	8	35.3	1.4	1	0.000867	2.6	17.51	0.45
	SCHEI1@21	374	8393	22	0.0056	12	6.6	0.6	2	0.000888	1.9	17.93	0.34
	SCHEI1@22	473	5055	11	0.0030	16	3.2	3.0	2	0.000878	3.3	17.75	0.58
	SCHEI1@23	285	24673	87	0.0105	13	20.4	0.9	1	0.000902	2.2	18.22	0.39
	SCHEI1@24	356	7599	21	0.0045	14	6.2	0.6	1	0.000873	1.8	17.64	0.31
	SCHEI1@28	290	22331	77	0.0156	10	19.3	0.8	2	0.000863	1.7	17.44	0.29
	SCHEI1@29	252	15566	62	0.0177	10	13.2	2.3	3	0.000885	2.5	17.88	0.45
	SCHEI1@31	170	11071	65	0.0151	13	16.4	1.7	2	0.000874	3.1	17.65	0.55
B	**SCHEI1@10**	880	19122	22	0.0145	14	5.9	1.6	9	0.000805	3.9	16.27	0.64

https://doi.org/10.5194/se-2019-162
Preprint. Discussion started: 30 October 2019

	SCHEI1@27	361	7525	21	0.0056	11	6.2	0.6	3	0.000825	1.8	16.66	0.30
	SCHEI1@33	130	1711	13	0.0028	19	4.0	1.6	1	0.000827	2.8	16.72	0.47
	SCHEI1@34	284	2432	9	0.0012	33	2.5	1.4	1	0.000791	2.6	15.97	0.42
	SCHEI1@05	*611*	*13815*	*23*	*0.0142*	*12*	*5.0*	*3.8*	*11*	*0.000984*	*3.7*	*19.87*	*0.74*
	SCHEI1@06	*582*	*7312*	*13*	*0.0134*	*14*	*3.4*	*1.7*	*15*	*0.001029*	*3.9*	*20.78*	*0.81*
	SCHEI1@07	*307*	*11197*	*36*	*0.0211*	*11*	*7.8*	*4.3*	*10*	*0.000949*	*3.1*	*19.17*	*0.59*
	SCHEI1@08	*651*	*7831*	*12*	*0.0122*	*12*	*3.3*	*1.0*	*14*	*0.000976*	*2.6*	*19.72*	*0.52*
	SCHEI1@09	*638*	*8160*	*13*	*0.0096*	*15*	*3.4*	*1.1*	*11*	*0.000993*	*3.1*	*20.07*	*0.63*
	SCHEI1@15	*304*	*23791*	*78*	*0.0346*	*8*	*11.4*	*4.1*	*12*	*0.000946*	*1.5*	*19.12*	*0.29*
	SCHEI1@30	*289*	*7594*	*26*	*0.0097*	*11*	*7.9*	*3.8*	*2*	*0.000882*	*7.2*	*17.81*	*1.27*
	SCHEI1@32	*154*	*27431*	*178*	*0.0270*	*9*	*30.7*	*3.8*	*2*	*0.000949*	*4.9*	*19.17*	*0.93*
A	**GART1@07**	184	10255	56	0.0119	12	13.5	3.3	2	0.000838	2.5	16.94	0.43
	GART1@08	242	7025	29	0.0130	10	7.7	0.9	5	0.000816	2.0	16.49	0.33
	GART1@09	120	8906	75	0.0133	12	16.8	1.4	2	0.000824	1.7	16.65	0.28
	GART1@10	195	16473	84	0.0233	9	20.8	1.7	2	0.000843	1.6	17.03	0.27
	GART1@11	230	11085	48	0.0117	15	11.9	1.2	3	0.000829	1.8	16.75	0.31
	GART1@22	56	3414	61	0.0210	10	11.4	1.9	6	0.000882	2.0	17.82	0.35
	GART1@23	93	6114	66	0.0223	10	12.2	2.3	6	0.000848	1.2	17.13	0.20
	GART1@24	92	5081	55	0.0237	10	10.7	1.2	7	0.000853	2.1	17.22	0.36
	GART1@25	100	6215	62	0.0229	11	12.1	1.2	6	0.000845	1.9	17.07	0.33
	GART1@26	90	6437	71	0.0193	11	12.7	2.1	6	0.000838	1.9	16.92	0.32
B	**GART1@01**	8	4390	539	0.0514	11	25.8	4.5	6	0.000806	3.3	16.29	0.53
	GART1@02	8	6159	777	0.0771	18	21.6	9.8	8	0.000843	3.8	17.03	0.64
	GART1@04b	10	4380	451	0.0408	13	42.8	5.1	1	0.000821	1.8	16.58	0.30
	GART1@05	24	11128	470	0.0385	13	51.3	3.4	1	0.000824	1.6	16.65	0.27
	GART1@17	66	15613	236	0.0303	8	23.8	1.7	4	0.000857	1.2	17.32	0.21
	GART1@18	89	19136	215	0.0267	9	27.8	1.4	2	0.000822	1.3	16.62	0.22
	GART1@19	11	6736	635	0.0510	17	50.5	8.7	2	0.000830	2.2	16.77	0.36
	GART1@20	103	17378	168	0.0325	8	25.6	2.0	3	0.000854	2.0	17.26	0.35
	GART1@21	71	15659	219	0.0327	8	27.0	1.8	3	0.000847	1.6	17.11	0.27
	GART1@03	*7*	*3553*	*484*	*0.0507*	*5*	*3.3*	*7.7*	*64*	*0.001637*	*15.5*	*33.06*	*5.13*
	GART1@04	*3*	*1445*	*431*	*0.0485*	*8*	*4.3*	*9.4*	*49*	*0.001311*	*11.3*	*26.48*	*2.98*
	GART1@06	*214*	*118344*	*552*	*0.0211*	*28*	*49.3*	*2.9*	*1*	*0.000418*	*3.0*	*8.44*	*0.25*
A	**NOWA3@02**	57	6302	111	0.0380	8	9.4	5.4	15	0.000849	2.9	17.16	0.49
	NOWA3@03	38	5205	137	0.0276	11	16.8	5.8	7	0.000876	3.0	17.69	0.53
	NOWA3@22	72	3607	50	0.0121	20	14.9	1.6	1	0.000840	3.8	16.98	0.65
	NOWA3@23	61	5010	81	0.0142	18	18.8	1.5	3	0.000904	2.5	18.26	0.46
	NOWA3@24	86	7377	86	0.0235	16	21.9	1.7	3	0.000804	2.3	16.25	0.38
	NOWA3@25	53	4052	77	0.0145	20	20.1	1.6	2	0.000837	1.8	16.91	0.31

https://doi.org/10.5194/se-2019-162
Preprint. Discussion started: 30 October 2019

B	**NOWA3@17**	59	3023	51	0.0125	13	9.4	3.8	6	0.000864	2.9	17.46	0.51
	NOWA3@18	53	2550	48	0.0180	10	8.6	4.3	7	0.000854	2.4	17.26	0.41
	NOWA3@19	60	4084	68	0.0181	10	11.7	3.8	5	0.000876	3.1	17.70	0.54
	NOWA3@20	57	3304	58	0.0183	10	10.4	3.6	6	0.000862	2.3	17.42	0.40
	NOWA3@21	86	2990	35	0.0187	20	7.2	11.7	12	0.000794	4.9	16.04	0.79
C	**NOWA3@12**	17	6374	375	0.0381	9	17.0	10.6	7	0.000894	2.7	18.05	0.49
	NOWA3@13	12	5354	436	0.0422	10	18.7	10.6	7	0.000884	3.9	17.87	0.69
	NOWA3@14	14	5563	406	0.0405	10	18.0	9.0	7	0.000830	3.4	16.76	0.56
	NOWA3@15	15	5438	367	0.0343	12	20.1	9.1	6	0.000835	3.1	16.87	0.52
	NOWA3@16	21	8142	389	0.0351	11	17.3	8.3	8	0.000817	3.4	16.51	0.56
	NOWA3@01	*36*	*3097*	*87*	*0.0222*	*12*	*11.2*	*6.5*	*9*	*0.000948*	*4.6*	*19.16*	*0.89*
	NOWA3@04	*16*	*1755*	*110*	*0.0432*	*6*	*5.1*	*7.7*	*36*	*0.001106*	*8.1*	*22.34*	*1.81*
	NOWA3@05	*38*	*2906*	*76*	*0.0412*	*7*	*4.8*	*7.4*	*36*	*0.001117*	*7.5*	*22.56*	*1.70*
	NOWA3@06	*70*	*5640*	*81*	*0.0305*	*12*	*7.0*	*6.5*	*21*	*0.000956*	*6.2*	*19.31*	*1.19*
	NOWA3@07	*47*	*1227*	*26*	*0.0244*	*9*	*4.1*	*4.9*	*25*	*0.001069*	*6.8*	*21.59*	*1.46*
	NOWA3@08	*61*	*806*	*13*	*0.0194*	*13*	*3.1*	*2.6*	*27*	*0.001176*	*7.5*	*23.76*	*1.79*
	NOWA3@09	*71*	*1048*	*15*	*0.0284*	*13*	*3.1*	*3.3*	*33*	*0.001149*	*7.3*	*23.22*	*1.68*
	NOWA3@10	*59*	*1367*	*23*	*0.0244*	*16*	*3.9*	*3.4*	*28*	*0.001044*	*7.2*	*21.10*	*1.51*
	NOWA3@11	*28*	*1787*	*64*	*0.0269*	*9*	*6.9*	*7.0*	*16*	*0.001026*	*5.4*	*20.72*	*1.11*
A	**GART3@13**	48	5272	111	0.0314	12	10.0	7.4	13	0.000904	4.4	18.27	0.81
	GART3@14	72	8521	118	0.0423	13	10.6	6.8	12	0.000863	3.7	17.44	0.64
	GART3@15	57	6233	110	0.0351	12	8.5	7.6	17	0.001000	4.4	20.19	0.88
	GART3@16	69	8123	118	0.0327	12	8.0	9.6	17	0.000960	6.0	19.39	1.17
	GART3@17	181	21273	118	0.0278	19	7.1	8.7	21	0.000873	7.2	17.63	1.28
	GART3@18	140	13707	98	0.0405	15	6.6	8.3	23	0.000872	6.5	17.62	1.15
B	**GART3@07**	118	5705	49	0.0221	18	8.9	4.4	7	0.000894	2.8	18.07	0.51
	GART3@08	220	8924	41	0.0239	13	6.2	4.5	13	0.000842	5.4	17.02	0.91
	GART3@09	415	14316	35	0.0181	14	5.5	4.1	15	0.000875	4.9	17.67	0.87
	GART3@10	191	7999	42	0.0223	13	6.1	5.7	13	0.000843	3.6	17.04	0.62
	GART3@11	281	13310	47	0.0219	16	7.2	4.3	9	0.000803	4.0	16.23	0.65
	GART3@12	698	39570	57	0.0291	17	7.9	5.7	11	0.000783	3.8	15.82	0.60
	GART3@21	161	10194	63	0.0294	15	8.8	6.4	10	0.000956	4.3	19.30	0.82
	GART3@22	1030	49325	48	0.0208	19	6.4	5.7	17	0.000866	4.8	17.51	0.83
	GART3@23	194	11748	60	0.0295	12	8.4	4.9	11	0.000884	3.3	17.86	0.58
C	**GART3@01**	60	3329	55	0.0211	16	8.9	5.9	8	0.000811	3.9	16.39	0.64
	GART3@03	137	4939	36	0.0344	16	4.5	5.7	19	0.000783	6.9	15.83	1.09
	GART3@04	135	4025	30	0.0244	18	3.9	4.4	22	0.000814	8.2	16.45	1.36
	GART3@05	62	3163	51	0.0240	17	5.8	6.0	14	0.000810	7.5	16.38	1.23
	GART3@06	108	5220	49	0.0232	19	5.4	7.2	15	0.000750	5.6	15.15	0.85
	GART3@02	*42*	*927*	*22*	*0.0119*	*45*	*4.4*	*9.0*	*16*	*0.001049*	*17.9*	*21.20*	*3.78*

https://doi.org/10.5194/se-2019-162
Preprint. Discussion started: 30 October 2019

GART3@19	*76*	*3055*	*40*	*0.0334*	*14*	*4.6*	*7.0*	*27*	*0.001129*	*7.7*	*22.81*	*1.75*
GART3@20	*187*	*3428*	*18*	*0.0216*	*19*	*3.6*	*4.2*	*25*	*0.001001*	*7.9*	*20.22*	*1.59*
STEI2@01	265	9618	36	0.0068	13	10.0	0.8	2	0.000894	2.0	18.06	0.36
STEI2@02	265	9882	37	0.0076	12	10.2	0.8	2	0.000858	1.7	17.34	0.29
STEI2@03	333	12059	36	0.0092	11	10.5	0.8	2	0.000867	1.6	17.51	0.27
STEI2@04	258	11350	44	0.0084	12	12.2	0.8	1	0.000846	2.4	17.09	0.41
STEI2@05	279	5706	20	0.0062	15	5.7	1.0	2	0.000843	2.0	17.03	0.34
STEI2@06	192	3681	19	0.0077	15	5.5	2.4	4	0.000906	2.9	18.31	0.54
STEI2@07	131	2676	20	0.0090	14	5.5	1.1	6	0.000878	2.4	17.73	0.42
STEI2@08	229	3096	13	0.0053	16	4.1	1.7	3	0.000890	4.5	17.98	0.81
STEI2@09	303	3070	10	0.0045	17	3.1	1.1	3	0.000892	3.9	18.03	0.70
STEI2@10	195	3848	20	0.0069	16	5.5	2.3	3	0.000873	3.0	17.65	0.53
STEI2@11	230	4018	17	0.0045	17	5.4	1.0	2	0.000898	1.7	18.14	0.31
STEI2@12	366	7338	20	0.0068	11	5.7	0.8	3	0.000856	2.5	17.30	0.43
STEI2@13	407	6516	16	0.0054	13	4.8	0.9	3	0.000877	2.3	17.73	0.40
STEI2@14	360	5666	16	0.0057	12	4.8	0.8	3	0.000868	1.9	17.53	0.33
STEI2@15	229	12353	54	0.0121	11	14.0	0.8	2	0.000846	1.5	17.09	0.25
STEI2@16	233	5052	22	0.0077	12	6.0	0.9	3	0.000866	1.5	17.50	0.26
STEI2@17	223	4150	19	0.0062	14	5.5	1.0	2	0.000864	2.1	17.46	0.37
STEI2@18	356	6216	17	0.0075	15	9.9	1.0	1	0.000868	1.9	17.54	0.34
STEI2@19	212	6475	31	0.0082	14	9.3	0.9	1	0.000918	1.7	18.55	0.32
STEI2@20	231	4632	20	0.0061	16	6.1	1.0	1	0.000883	2.6	17.83	0.45
Eastern Tauern Window												
ORT1@01	158	1998	13	0.0032	20	3.9	1.1	2	0.001002	1.7	20.25	0.34
ORT1@02	241	2890	12	0.0041	19	3.6	1.2	2	0.001013	3.0	20.47	0.61
ORT1@03	150	2371	16	0.0045	18	4.6	1.2	2	0.001032	3.0	20.84	0.62
ORT1@04	177	2269	13	0.0041	18	3.9	1.2	2	0.000966	2.8	19.52	0.55
ORT1@05	65	1902	29	0.0075	18	7.3	1.8	3	0.001005	2.6	20.31	0.53
ORT1@07	113	2015	18	0.0150	10	4.5	1.2	13	0.000992	3.0	20.05	0.60
ORT1@08	104	2580	25	0.0120	13	5.9	2.2	8	0.001009	2.3	20.38	0.47
ORT1@09	105	2251	21	0.0082	16	5.9	1.2	4	0.000995	1.8	20.11	0.37
ORT1@10	124	3755	30	0.0235	7	5.8	1.7	16	0.000972	4.3	19.64	0.84
ORT1@11	64	1919	30	0.0096	20	7.1	3.5	4	0.001017	3.2	20.54	0.67
ORT1@12	84	2984	35	0.0109	29	8.3	3.9	4	0.001046	3.1	21.12	0.66
ORT1@13	57	3367	59	0.0166	16	11.9	4.8	3	0.000958	2.5	19.36	0.49
ORT1@14	48	1917	40	0.0138	17	8.5	2.9	4	0.000970	2.8	19.59	0.54
ORT@06	*101*	*1408*	*14*	*0.0089*	*14*	*3.7*	*2.6*	*7*	*0.001110*	*5.0*	*22.42*	*1.12*
ORT@15	*70*	*3070*	*44*	*0.0194*	*12*	*7.8*	*9.0*	*10*	*0.001317*	*6.0*	*26.60*	*1.61*
A **HOAR1@01**	33	657	20	0.0154	21	5.0	2.6	9	0.001121	4.5	22.64	1.02

https://doi.org/10.5194/se-2019-162
Preprint. Discussion started: 30 October 2019

	HOAR1@02	49	874	18	0.0208	19	4.2	2.9	14	0.001233	7.6	24.91	1.89
	HOAR1@03	43	742	17	0.0159	18	4.2	2.4	8	0.001142	5.8	23.08	1.34
	HOAR1@04	72	1046	15	0.0139	19	3.5	2.4	9	0.001166	5.4	23.56	1.26
	HOAR1@06	92	1120	12	0.0096	21	3.6	1.8	7	0.001155	5.4	23.33	1.26
	HOAR1@07	78	1387	18	0.0092	18	4.1	3.5	7	0.000962	6.8	19.43	1.32
	HOAR1@08	65	1395	21	0.0144	19	4.9	3.4	10	0.001086	4.0	21.94	0.87
	HOAR1@09	45	1229	27	0.0122	23	6.0	3.2	5	0.001171	5.7	23.65	1.34
	HOAR1@10	231	1462	6	0.0050	18	2.2	1.5	5	0.001154	3.4	23.31	0.78
	HOAR1@11	43	4153	97	0.0229	13	18.7	3.6	2	0.001063	2.2	21.47	0.48
	HOAR1@12	79	2012	25	0.0176	12	5.3	2.5	15	0.001026	3.5	20.73	0.72
	HOAR1@13	92	3234	35	0.0099	18	7.6	1.5	4	0.001026	2.0	20.72	0.41
	HOAR1@14	101	2022	20	0.0127	15	4.4	1.6	8	0.001196	5.9	24.16	1.43
	HOAR1@16	110	2116	19	0.0071	18	4.8	2.4	4	0.001081	3.7	21.83	0.80
	HOAR1@17	71	1327	19	0.0159	18	4.5	3.1	9	0.001192	2.1	24.08	0.50
	HOAR1@18	52	998	19	0.0145	17	4.9	2.0	7	0.001232	4.7	24.88	1.16
	HOAR1@19	33	578	18	0.0117	20	4.6	2.2	10	0.001258	4.8	25.41	1.23
	HOAR1@20	44	1341	31	0.0140	18	7.0	3.3	5	0.001133	2.3	22.89	0.53
	HOAR1@21	24	519	21	0.0213	18	4.6	3.4	14	0.001018	7.0	20.57	1.44
	HOAR1@22	38	1303	34	0.0243	22	6.5	5.3	10	0.001172	4.2	23.68	1.01
	HOAR1@23	124	1853	15	0.0050	25	4.2	1.8	4	0.001103	5.0	22.29	1.12
	HOAR1@24	75	1863	25	0.0110	19	5.6	2.8	4	0.001007	5.7	20.35	1.16
	HOAR1@25	38	1117	30	0.0148	20	5.9	4.2	8	0.001084	4.4	21.89	0.95
	HOAR1@26	42	936	22	0.0139	20	5.0	2.3	8	0.001106	5.6	22.33	1.25
	HOAR1@27	110	1200	11	0.0103	15	2.9	2.4	13	0.001048	4.8	21.18	1.01
	HOAR@28	75	997	13	0.0169	13	2.9	1.8	17	0.001122	4.2	22.66	0.95
B	**HOAR1@29**	61	14974	246	0.0334	10	45.6	2.9	1	0.001017	1.6	20.55	0.32
	HOAR1@30	59	424	7	0.0102	20	2.2	2.7	15	0.001173	5.7	23.70	1.34
	HOAR1@31	101	2404	24	0.0107	16	5.6	3.4	5	0.000984	3.0	19.87	0.60
	HOAR1@05	*56*	*469*	*8*	*0.0106*	*22*	*2.4*	*2.7*	*14*	*0.001146*	*9.9*	*23.15*	*2.30*
	HOAR1@15	*78*	*2391*	*31*	*0.0331*	*10*	*4.2*	*6.7*	*28*	*0.001558*	*7.9*	*31.46*	*2.49*
	HOAR1@32	*258*	*691*	*3*	*0.0052*	*16*	*1.1*	*3.1*	*18*	*0.001371*	*5.3*	*27.69*	*1.46*
	MOKR1@08	301	4676	16	0.0116	19	4.0	3.6	10	0.001075	6.6	21.72	1.44
	MOKR1@09	745	4767	6	0.0059	17	2.0	1.1	8	0.001096	5.7	22.13	1.26
	MOKR1@12	1039	21019	20	0.0146	18	4.0	3.9	9	0.001016	8.0	20.53	1.64
A	**MOKR1@19**	113	1329	12	0.0000	100	3.3	3.5	2	0.001019	5.9	20.58	1.22
	MOKR1@21	555	10097	18	0.0049	58	4.9	2.9	0	0.000978	7.8	19.75	1.55
	MOKR1@22	674	13678	20	0.0022	100	6.3	3.4	0	0.001130	4.8	22.82	1.09
	MOKR1@23	180	1454	8	0.0043	50	2.1	2.8	6	0.000920	6.8	18.58	1.27
	MOKR1@24	270	3536	13	0.0010	71	3.8	2.5	1	0.000989	4.0	19.99	0.81

https://doi.org/10.5194/se-2019-162
Preprint. Discussion started: 30 October 2019

	MOKR1@25	220	2486	11	0.0025	71	3.8	2.7	2	0.000997	5.7	20.14	1.14
	MOKR1@26	88	1243	14	0.0066	41	4.3	2.4	3	0.000986	4.7	19.92	0.93
	MOKR1@27	306	3905	13	0.0054	58	3.4	3.3	4	0.000988	4.0	19.97	0.80
	MOKR1@28	473	6458	14	0.0028	71	4.4	2.7	1	0.001007	5.0	20.35	1.02
	MOKR1@29	335	1656	5	0.0021	58	1.8	2.3	3	0.001087	5.5	21.96	1.20
	MOKR1@30	645	4273	7	0.0023	58	1.9	2.3	2	0.000867	8.1	17.52	1.42
	MOKR1@31	660	4778	7	0.0008	100	2.4	2.3	1	0.001080	3.2	21.82	0.69
	MOKR1@20	569	4689	8	0.0060	50	1.5	3.5	1	0.000709	6.5	14.33	0.93
B	**MOKR1@01**	95	17647	186	0.0321	11	24.9	8.2	2	0.001055	3.1	21.31	0.66
	MOKR1@02	118	16628	140	0.0232	14	22.3	5.9	2	0.001058	3.0	21.37	0.65
	MOKR1@03	109	17066	156	0.0253	15	22.4	7.2	2	0.001030	2.8	20.82	0.57
	MOKR1@04	116	12424	107	0.0215	14	16.0	7.8	4	0.001063	3.4	21.47	0.73
	MOKR1@05	111	7533	68	0.0225	14	11.0	6.6	5	0.001076	4.1	21.73	0.90
	MOKR1@06	177	8755	49	0.0172	22	8.9	5.8	4	0.001011	2.9	20.43	0.59
	MOKR1@13	92	13514	147	0.0279	13	18.4	8.7	4	0.001051	2.8	21.23	0.59
	MOKR1@14	214	10182	48	0.0110	26	10.1	3.6	3	0.000975	3.5	19.70	0.69
	MOKR1@15	285	12267	43	0.0132	15	9.2	4.3	3	0.000981	3.2	19.83	0.63
	MOKR1@16	362	13672	38	0.0137	16	8.6	3.5	3	0.000946	3.8	19.11	0.73
	MOKR1@17	92	12153	132	0.0198	16	18.5	7.7	3	0.001068	3.3	21.57	0.71
	MOKR1@18	294	12047	41	0.0176	19	7.1	5.2	9	0.000923	4.5	18.65	0.83
	MOKR1@07	*216*	*2127*	*10*	*0.0114*	*15*	*2.7*	*2.7*	*13*	*0.001326*	*8.2*	*26.79*	*2.20*
	MOKR1@10	*569*	*1613*	*3*	*0.0043*	*33*	*1.1*	*2.5*	*17*	*0.001335*	*8.9*	*26.96*	*2.39*
	MOKR1@11	*2861*	*8368*	*3*	*0.0066*	*22*	*1.0*	*2.8*	*17*	*0.001149*	*10.6*	*23.21*	*2.45*
A	**SAND1@10**	462	1988	4	0.0095	18	1.4	2.2	21	0.001203	6.6	24.29	1.60
	SAND1@12	1027	6008	6	0.0072	21	1.8	1.4	13	0.001070	5.9	21.61	1.26
	SAND1@13	295	1163	4	0.0052	30	1.3	1.8	16	0.001143	6.2	23.09	1.43
	SAND1@14	1034	6916	7	0.0129	19	1.8	1.7	19	0.000982	4.4	19.84	0.86
	SAND1@27	131	280	2	0.0000	100	0.7	3.5	7	0.001032	5.3	20.86	1.11
B	**SAND1@04**	100	5283	53	0.0339	20	6.5	6.2	14	0.001183	5.7	23.90	1.36
	SAND1@05	335	8637	26	0.0246	20	5.2	3.9	12	0.001189	6.0	24.02	1.44
	SAND1@06	701	18108	26	0.0239	21	5.3	4.0	12	0.001227	4.9	24.79	1.21
	SAND1@07	142	3852	27	0.0193	15	5.1	4.5	11	0.001058	3.8	21.37	0.81
	SAND1@08	116	4235	37	0.0176	18	6.8	4.0	8	0.000956	3.0	19.32	0.58
	SAND1@21	80	2989	37	0.0047	58	11.2	2.8	1	0.001059	2.4	21.39	0.51
	SAND1@22	395	15527	39	0.0080	58	9.3	3.6	1	0.001054	3.9	21.28	0.83
	SAND1@23	582	19958	34	-0.0030	100	7.5	3.8	2	0.000851	6.5	17.19	1.12
	SAND1@24	459	15793	34	0.0050	71	8.6	3.6	1	0.001006	3.6	20.33	0.74
	SAND1@25	429	14440	34	0.0055	71	11.1	3.7	1	0.001202	3.7	24.27	0.91
	SAND1@26	385	11752	31	0.0074	58	10.2	3.4	2	0.001060	4.8	21.42	1.04

https://doi.org/10.5194/se-2019-162
Preprint. Discussion started: 30 October 2019

SAND1@01	*43*	*869*	*20*	*0.0296*	*18*	*3.9*	*5.6*	*17*	*0.001292*	*9.8*	*26.09*	*2.54*
SAND1@02	*77*	*2191*	*28*	*0.0247*	*22*	*4.6*	*6.2*	*21*	*0.001273*	*9.5*	*25.72*	*2.45*
SAND1@09	*159*	*536*	*3*	*0.0052*	*28*	*1.3*	*3.2*	*21*	*0.001327*	*10.2*	*26.79*	*2.74*
SAND1@11	*1504*	*8278*	*6*	*0.0063*	*39*	*1.3*	*1.9*	*29*	*0.001213*	*14.0*	*24.51*	*3.42*
SAND1@15	*84*	*329*	*4*	*0.0244*	*13*	*1.4*	*3.3*	*43*	*0.001342*	*14.2*	*27.11*	*3.86*
SAND1@16	*122*	*319*	*3*	*0.0164*	*18*	*1.2*	*4.2*	*54*	*0.001267*	*20.6*	*25.58*	*5.27*
SAND1@17	*110*	*190*	*2*	*0.0182*	*18*	*1.0*	*5.0*	*66*	*0.001236*	*26.6*	*24.97*	*6.64*
SAND1@18	*156*	*800*	*5*	*0.0201*	*18*	*1.7*	*2.1*	*37*	*0.001299*	*10.5*	*26.24*	*2.76*
SAND1@19	*194*	*631*	*3*	*0.0174*	*18*	*1.4*	*4.1*	*48*	*0.001300*	*15.5*	*26.26*	*4.08*
SAND1@20	*174*	*309*	*2*	*0.0128*	*24*	*1.0*	*5.5*	*65*	*0.001296*	*25.4*	*26.17*	*6.64*
SAND1@28	*458*	*745*	*2*	*0.0012*	*100*	*0.6*	*4.0*	*7*	*0.001146*	*9.6*	*23.16*	*2.23*
SAND1@29	*520*	*530*	*1*	*0.0035*	*71*	*0.4*	*5.7*	*5*	*0.001228*	*9.2*	*24.80*	*2.27*
SAND1@30	*1538*	*1261*	*1*	*0.0019*	*100*	*0.4*	*6.1*	*8*	*0.001287*	*12.5*	*26.00*	*3.24*
SAND1@31	*1517*	*1851*	*1*	*0.0035*	*71*	*0.3*	*6.1*	*5*	*0.000836*	*13.3*	*16.88*	*2.25*
SAND1@32	*636*	*821*	*1*	*0.0015*	*100*	*0.0*	*14.2*	*-186*	*0.000225*	*61.6*	*4.55*	*2.80*
SAND1@33	*3581*	*1704*	*0*	*0.0000*	*100*	*0.1*	*18.1*	*-53*	*0.000508*	*36.3*	*10.26*	*3.73*
SAND1@34	*12906*	*11465*	*1*	*0.0000*	*100*	*0.0*	*24.7*	*-115*	*0.000250*	*41.1*	*5.05*	*2.07*
SAND1@35	*5033*	*9445*	*2*	*0.0000*	*100*	*0.4*	*5.9*	*5*	*0.000952*	*11.8*	*19.23*	*2.26*
SAND1@36	*2883*	*2921*	*1*	*0.0000*	*100*	*0.4*	*9.7*	*9*	*0.001178*	*21.9*	*23.80*	*5.22*
REIS1@17	76	134	2	0.0009	35	0.5	2.6	4	0.000783	10.5	15.82	1.66
REIS1@18	40	52	1	0.0008	45	0.4	3.5	9	0.000782	12.4	15.81	1.96
REIS1@19	71	96	1	0.0011	38	0.4	3.4	11	0.000793	8.6	16.02	1.38
REIS1@20	56	104	2	0.0003	71	0.5	3.1	7	0.000754	8.5	15.24	1.29
REIS1@21	39	52	1	0.0012	38	0.4	3.5	8	0.000884	6.7	17.86	1.19
REIS1@22	126	68	1	0.0006	33	0.1	3.7	9	0.000720	13.3	14.55	1.93
REIS1@24	39	65	2	0.0008	71	0.5	4.6	8	0.000824	10.6	16.64	1.77
REIS1@27	19	54	3	0.0051	27	0.9	3.4	12	0.000921	8.6	18.61	1.60
REIS1@28	59	302	5	0.0025	33	1.7	2.3	5	0.000918	4.6	18.54	0.85
REIS1@29	30	138	5	0.0024	45	1.2	3.6	9	0.000722	10.0	14.59	1.45
REIS1@31	28	128	5	0.0052	28	1.3	3.1	13	0.000852	10.2	17.21	1.75
REIS1@32	62	448	7	0.0028	26	2.4	1.7	1	0.001057	4.7	21.34	1.00
REIS1@33	161	158	1	0.0004	50	0.3	3.0	2	0.000801	5.2	16.19	0.85
REIS1@30	79	195	2	0.0027	45	0.6	5.3	16	0.000502	13.6	10.14	1.38
REIS1@23	*26*	*32*	*1*	*0.0013*	*50*	*0.4*	*4.7*	*3*	*0.000968*	*11.7*	*19.55*	*2.30*
REIS1@25	*26*	*27*	*1*	*0.0011*	*58*	*0.3*	*5.5*	*11*	*0.000913*	*14.5*	*18.44*	*2.68*
REIS1@26	*24*	*24*	*1*	*0.0015*	*50*	*0.3*	*6.3*	*25*	*0.000617*	*16.9*	*12.46*	*2.10*
REIS1@34	*101*	*66*	*1*	*0.0005*	*50*	*0.2*	*6.3*	*-4*	*0.000975*	*16.7*	*19.70*	*3.28*
REIS1@35	*27*	*71*	*3*	*0.0034*	*33*	*1.0*	*5.2*	*9*	*0.000988*	*13.7*	*19.95*	*2.74*
REIS1@36	*27*	*115*	*4*	*0.0056*	*29*	*1.2*	*5.2*	*17*	*0.000784*	*15.8*	*15.85*	*2.51*

https://doi.org/10.5194/se-2019-162
Preprint. Discussion started: 30 October 2019

***Table 4**: Th-U-Pb analyses of monazite by ion microprobe (Nordsim). Analyses resulting in unreliable dates (e.g. presence of cracks, affected by Pbc causing high uncertainty) were not considered and are written in italic.*

Groups	Analysis ID	U (ppm)	Th (ppm)	Th/U	$^{208}Pb/^{204}Pb$	1σ (%)	f208 (%)	204 and $ThNdO_2$ - corr $^{208}Pb/^{232}Th$	1σ (%)	204 and $ThNdO_2$ - corr spot ages $^{232}Th/^{208}Pb$ Age (Ma)	1σ (abs.)
Western Tauern Window											
A	**SCHR1@01**	423	37708	89	1660	6.030	1	0.001009	2.16	20.39	0.44
	SCHR1@02	499	36495	73	2195	7.506	1	0.001005	2.49	20.29	0.51
	SCHR1@03	417	45163	108	2042	5.480	1	0.001080	2.16	21.82	0.47
	SCHR1@04	438	43245	99	1916	5.841	1	0.001034	2.15	20.90	0.45
	SCHR1@05	465	37059	80	2179	6.894	1	0.001005	2.16	20.29	0.44
	SCHR1@06	443	46170	104	1856	7.549	1	0.001051	2.18	21.23	0.46
B	**SCHR1@07**	509	24001	47	1166	7.820	3	0.001009	2.13	20.38	0.43
	SCHR1@08	482	25025	52	1164	6.472	2	0.001033	2.16	20.87	0.45
	SCHR1@09	478	26320	55	1157	5.686	3	0.001012	2.14	20.45	0.44
	SCHR1@10	510	28255	55	1213	6.190	2	0.001027	2.13	20.74	0.44
	SCHR1@11	465	26453	57	1140	5.981	2	0.001053	2.14	21.28	0.46
	SCHR1@12	331	27180	82	1098	5.589	2	0.001018	2.13	20.57	0.44
	SCHR1@13	312	28957	93	1243	5.712	2	0.001028	2.14	20.76	0.45
	SCHR1@14	316	29632	94	1285	5.676	2	0.001006	2.18	20.32	0.44
	SCHR1@15	331	31105	94	1204	5.478	2	0.000994	2.17	20.08	0.44
	SCHR1@16	471	25641	54	1786	8.371	1	0.001005	2.16	20.30	0.44
	SCHR1@17	477	28482	60	1417	6.339	2	0.001002	2.17	20.25	0.44
	SCHR1@18	480	18234	38	1595	10.102	2	0.000976	2.17	19.71	0.43
	SCHR1@19	492	18252	37	1340	7.780	2	0.000979	2.17	19.78	0.43
	SCHR1@20	506	18432	36	1457	8.553	2	0.000972	2.22	19.63	0.43
	SCHR1@21	443	21802	49	1574	7.553	2	0.000979	2.16	19.78	0.43
	SCHR1@22	453	24816	55	1475	7.051	2	0.000991	2.15	20.03	0.43
C	**SCHR1@23**	211	16187	77	925	10.427	4	0.000957	2.37	19.34	0.46
	SCHR1@24	306	17861	58	541	6.558	6	0.000964	2.30	19.47	0.45
	SCHR1@25	363	17322	48	548	8.976	7	0.000968	2.56	19.56	0.50
	SCHR1@26	447	17105	38	1584	11.493	2	0.001027	3.23	20.74	0.67
	SCHR1@27	351	18354	52	1639	10.279	2	0.000954	2.71	19.28	0.52
	SCHR1@28	499	18145	36	1491	11.348	3	0.001005	3.14	20.30	0.64
A	**PFIT1@12**	103	11683	114	552	7.242	5	0.000806	2.14	16.29	0.35

https://doi.org/10.5194/se-2019-162
Preprint. Discussion started: 30 October 2019

	PFIT1@13	112	18466	165	580	5.227	5	0.000844	2.20	17.06	0.37
	PFIT1@14	117	13986	120	569	5.762	5	0.000868	2.23	17.54	0.39
	PFIT1@15	104	13449	130	471	5.005	7	0.000835	2.29	16.86	0.39
	PFIT1@16	65	15956	244	692	5.569	3	0.000882	2.21	17.82	0.39
	PFIT1@17	78	13368	171	582	6.586	5	0.000832	2.19	16.82	0.37
	PFIT1@18	79	12054	153	659	7.974	4	0.000858	2.37	17.34	0.41
	PFIT1@19	121	9937	82	701	9.961	5	0.000854	2.17	17.25	0.37
	PFIT1@20	119	8358	70	823	11.220	4	0.000850	2.18	17.18	0.37
B	**PFIT1@06**	245	5464	22	522	10.559	5	0.000665	2.27	13.44	0.31
	PFIT1@07	336	4523	13	414	10.687	8	0.000648	2.37	13.09	0.31
	PFIT1@08	347	3300	10	365	11.509	9	0.000659	2.37	13.32	0.32
	PFIT1@09	383	3220	8	344	12.713	10	0.000636	2.49	12.85	0.32
	PFIT1@10	388	2889	*7*	238	11.187	14	0.000633	2.73	12.80	0.35
	PFIT1@01	*30*	*5962*	*199*	*752*	*11.515*	*5*	*0.000628*	*2.27*	*12.70*	*0.29*
	PFIT1@02	*32*	*6627*	*209*	*714*	*12.650*	*4*	*0.000720*	*2.27*	*14.56*	*0.33*
	PFIT1@03	*13*	*5940*	*466*	*1101*	*10.816*	*2*	*0.000809*	*2.24*	*16.34*	*0.37*
	PFIT1@04	*36*	*6027*	*166*	*849*	*15.037*	*3*	*0.000681*	*2.32*	*13.75*	*0.32*
	PFIT1@05	*84*	*8610*	*102*	*1381*	*18.957*	*3*	*0.000691*	*3.33*	*13.95*	*0.47*
	PFIT1@11	*110*	*13146*	*119*	*584*	*5.797*	*5*	*0.000758*	*2.10*	*15.31*	*0.32*

Central Tauern Window

	HOPF2@15	82	61530	749	721	3.580	3	0.000542	2.30	10.94	0.25
	HOPF2@16	69	33784	490	621	4.412	4	0.000619	2.28	12.51	0.29
	HOPF2@17	97	33439	343	971	6.810	3	0.000643	2.84	13.00	0.37
A	**HOPF2@18**	77	40713	530	271	3.881	13	0.000666	2.40	13.46	0.32
	HOPF2@19	120	62586	520	838	4.852	3	0.000605	3.40	12.23	0.42
	HOPF2@20	120	49522	413	854	9.922	4	0.000569	2.33	11.50	0.27
	HOPF2@21	173	37157	215	1305	13.395	3	0.000663	2.73	13.40	0.37
	HOPF2@07	49	28763	591	498	4.900	7	0.000560	2.14	11.31	0.24
	HOPF2@08	46	28779	627	509	4.500	6	0.000594	2.11	12.01	0.25
	HOPF2@09	55	32338	593	429	3.810	7	0.000603	2.06	12.18	0.25
B	**HOPF2@10**	76	22645	296	641	9.139	6	0.000598	3.49	12.09	0.42
	HOPF2@11	40	28273	701	142	8.000	25	0.000583	3.45	11.78	0.41
	HOPF2@12	38	26357	689	374	4.826	9	0.000634	2.08	12.81	0.27
	HOPF2@13	52	40578	775	299	6.194	11	0.000613	2.41	12.39	0.30
	HOPF2@14	55	27790	505	259	5.171	13	0.000613	2.07	12.38	0.26
	HOPF2@01	40	23096	582	680	7.463	4	0.000565	2.15	11.42	0.25
	HOPF2@02	42	25870	612	581	6.585	5	0.000587	2.17	11.87	0.26
C	**HOPF2@03**	45	29023	642	553	4.768	5	0.000618	2.20	12.49	0.27
	HOPF2@04	50	30246	610	508	4.728	5	0.000621	2.26	12.56	0.28
	HOPF2@05	57	32908	577	463	4.034	6	0.000629	2.36	12.70	0.30

https://doi.org/10.5194/se-2019-162
Preprint. Discussion started: 30 October 2019

	HOPF2@06	58	28865	500	480	4.524	6	0.000602	2.08	12.16	0.25
A	**KNOR1_@19**	149	12269	82	465	6.834	6	0.000526	2.30	10.64	0.24
	KNOR1_@20	181	9307	52	277	7.353	13	0.000512	3.04	10.34	0.31
	KNOR1_@21	239	9337	39	647	14.146	5	0.000574	3.59	11.60	0.42
	KNOR1_@22	172	8289	48	540	9.262	6	0.000534	2.67	10.78	0.29
	KNOR1_@24	194	7199	37	615	12.664	6	0.000515	3.08	10.40	0.32
B	**KNOR1_@01**	32	7767	246	194	5.350	19	0.000499	2.07	10.08	0.21
	KNOR1_@02	35	6107	175	202	6.264	18	0.000524	2.46	10.59	0.26
	KNOR1_@03	36	9885	273	114	4.841	33	0.000517	2.44	10.44	0.25
	KNOR1_@04	30	6902	234	93	3.382	41	0.000545	1.92	11.00	0.21
	KNOR1_@06	33	9203	277	171	4.416	21	0.000525	2.02	10.61	0.21
	KNOR1_@07	33	4983	152	112	4.810	33	0.000518	2.24	10.46	0.23
	KNOR1_@08	36	3783	105	136	5.985	26	0.000516	2.37	10.42	0.25
	KNOR1_@09	39	5846	149	302	7.354	11	0.000515	2.28	10.41	0.24
C	**KNOR1_@05**	27	9535	356	104	3.093	35	0.000565	1.93	11.41	0.22
	KNOR1_@10	48	5633	118	453	11.056	7	0.000501	2.40	10.13	0.24
	KNOR1_@11	48	4611	96	445	11.786	6	0.000525	2.59	10.62	0.28
	KNOR1_@12	57	4583	81	459	10.996	7	0.000502	2.24	10.15	0.23
	KNOR1_@13	54	4104	77	489	11.330	7	0.000504	2.33	10.18	0.24
	KNOR1_@14	56	6093	108	724	13.355	4	0.000493	2.22	9.96	0.22
	KNOR1_@15	76	6847	91	705	13.068	3	0.000511	2.26	10.33	0.23
	KNOR1_@16	65	5872	91	522	14.528	5	0.000503	2.36	10.16	0.24
	KNOR1_@18	77	8867	114	630	10.939	3	0.000541	2.55	10.93	0.28
	KNOR1_@17	73	6281	86	577	10.481	4	0.000564	2.28	11.40	0.26

Eastern Tauern Window

A	**KAIS6@29**	12	32285	2726	324	2.307	11	0.001014	2.41	20.48	0.49
	KAIS6@37	10	35152	3587	323	2.469	11	0.001065	2.44	21.51	0.52
	KAIS6@38	10	35481	3480	438	2.739	8	0.001048	2.54	21.17	0.54
	KAIS6@39	10	31600	3326	311	2.609	12	0.001020	2.44	20.60	0.50
	KAIS6@41	8	32642	4280	353	3.271	10	0.001058	2.50	21.36	0.53
	KAIS6@42	6	29873	4677	291	2.296	12	0.001053	2.38	21.27	0.51
B	**KAIS6@15**	5	21644	4568	142	1.779	26	0.001030	2.04	20.82	0.42
	KAIS6@16	5	22052	4771	161	1.922	23	0.001019	2.11	20.59	0.44
	KAIS6@17	5	25100	4752	186	1.993	20	0.001042	2.23	21.06	0.47
	KAIS6@18	5	25260	4905	148	1.871	25	0.001040	2.16	21.00	0.45
	KAIS6@19	5	23495	5173	147	2.169	25	0.001037	2.13	20.94	0.45
	KAIS6@20	5	24260	5377	155	1.894	24	0.001027	2.20	20.75	0.46
	KAIS6@21	5	25950	5040	158	1.971	24	0.001010	2.15	20.40	0.44

https://doi.org/10.5194/se-2019-162
Preprint. Discussion started: 30 October 2019

	KAIS6@22	4	20175	4625	136	1.915	27	0.001037	2.08	20.95	0.44
	KAIS6@23	3	18427	5349	153	2.062	24	0.001026	2.20	20.73	0.46
	KAIS6@24	4	17328	4822	178	2.255	20	0.001045	2.20	21.11	0.46
	KAIS6@25	5	17901	3588	154	2.266	24	0.001042	2.19	21.04	0.46
	KAIS6@26	4	19477	5281	165	2.214	22	0.001014	2.20	20.49	0.45
	KAIS6@27	4	19595	5290	165	2.205	22	0.001029	2.18	20.79	0.45
	KAIS6@28	3	17683	5368	167	2.225	22	0.001052	2.21	21.25	0.47
	KAIS6@31	3	19464	6314	208	2.462	18	0.001049	2.25	21.19	0.48
	KAIS6@32	3	17623	5729	145	2.047	26	0.001007	2.12	20.34	0.43
	KAIS6@33	4	23433	5395	190	2.027	19	0.001016	2.29	20.53	0.47
	KAIS6@34	3	22517	6923	175	1.970	21	0.001015	2.19	20.51	0.45
	KAIS6@35	4	23426	6129	178	1.965	21	0.001028	2.19	20.77	0.46
	KAIS6@36	4	24762	6924	170	2.304	22	0.001032	2.23	20.86	0.46
	KAIS6@43	4	19511	4948	229	2.717	15	0.001023	2.38	20.68	0.49
	KAIS6@44	5	20543	3995	247	3.160	15	0.001003	2.38	20.27	0.48
	KAIS6@45	4	17366	4418	219	2.782	16	0.001061	2.29	21.43	0.49
	KAIS6@46	4	14595	3614	231	3.427	16	0.001080	2.34	21.81	0.51
	KAIS6@01	2	13078	6002	83	2.339	46	0.001009	1.82	20.38	0.37
	KAIS6@02	3	14140	4835	97	1.984	39	0.001031	1.87	20.82	0.39
	KAIS6@05	3	10157	2957	98	2.228	39	0.001017	1.86	20.55	0.38
C	**KAIS6@06**	4	15227	3566	104	2.225	36	0.000994	1.99	20.08	0.40
	KAIS6@09	3	10348	3946	74	1.649	52	0.001026	1.56	20.74	0.32
	KAIS6@10	3	12624	4224	90	1.888	42	0.001036	1.78	20.92	0.37
	KAIS6@12	3	10457	3171	91	2.238	42	0.001019	1.83	20.58	0.38
	KAIS6@03	4	15947	3922	100	2.148	38	0.000941	1.98	19.02	0.38
	KAIS6@04	4	16156	3905	91	2.181	42	0.000889	2.10	17.96	0.38
	KAIS6@07	6	11981	2002	89	3.553	43	0.000886	2.26	17.91	0.40
	KAIS6@08	3	10466	3145	86	1.846	45	0.000949	1.71	19.16	0.33
D	**KAIS6@11**	4	13094	3210	89	2.393	44	0.000842	1.95	17.01	0.33
	KAIS6@13	4	13271	3273	88	2.913	44	0.000913	2.05	18.44	0.38
	KAIS6@14	9	13459	1568	105	3.955	37	0.000834	2.69	16.85	0.45
	KAIS6@30	14	25376	1840	229	2.365	16	0.000954	2.30	19.26	0.44
	KAIS6@40	10	32326	3141	293	2.801	12	0.000958	2.59	19.36	0.50
	KAIS6@47	9	31411	3692	312	3.664	11	0.000949	2.42	19.16	0.46
	KAIS6@48	*13*	*18728*	*1403*	*217*	*3.029*	*17*	*0.001013*	*2.29*	*20.47*	*0.47*
	KAIS6@49	*13*	*18241*	*1449*	*248*	*2.679*	*14*	*0.001070*	*2.34*	*21.62*	*0.51*
	SALZ18@01	11	443	40	426	9.205	7	0.000928	2.29	18.74	0.43
	SALZ18@02	19	11907	639	555	11.284	5	0.000919	2.20	18.56	0.41
	SALZ18@03	23	12452	552	1310	13.609	1	0.000853	2.29	17.24	0.39
	SALZ18@04	20	8334	407	796	10.141	4	0.000908	2.48	18.35	0.46

https://doi.org/10.5194/se-2019-162
Preprint. Discussion started: 30 October 2019

SALZ18@05	28	6912	245	1362	12.340	1	0.000903	2.22	18.24	0.40
SALZ18@06	11	2256	200	1192	13.398	1	0.000941	2.31	19.01	0.44
SALZ18@07	23	9797	429	2103	19.277	0	0.000860	2.37	17.37	0.41
SALZ18@08	20	4607	232	1047	14.480	3	0.000858	2.40	17.33	0.42
SALZ18@09	18	3952	224	1249	18.002	2	0.000928	2.47	18.75	0.46
SALZ18@10	19	3681	189	882	18.429	4	0.000883	2.62	17.85	0.47
SALZ18@11	13	1751	134	1043	14.785	2	0.000956	2.40	19.31	0.46
SALZ18@12	17	4555	267	809	18.979	4	0.000882	2.78	17.82	0.50
SALZ18@13	17	1752	106	625	26.861	6	0.000832	3.62	16.81	0.61
SALZ18@14	22	1037	48	901	10.946	2	0.000935	2.28	18.89	0.43
SALZ18@15	37	9684	262	1066	14.544	2	0.000779	2.40	15.73	0.38

A

LOHN4@01	14	14552	1076	79	2.725	48	0.001025	2.03	20.72	0.42
LOHN4@02	39	25804	662	266	3.804	14	0.000959	2.83	19.37	0.55
LOHN4@03	11	12883	1175	151	2.436	24	0.001025	2.12	20.72	0.44
LOHN4@04	16	16561	1017	170	3.810	22	0.001044	2.41	21.08	0.51
LOHN4@07	34	35456	1048	337	2.194	10	0.001094	2.42	22.10	0.53
LOHN4@08	31	32345	1044	312	2.170	11	0.001072	2.46	21.65	0.53
LOHN4@09	33	34180	1040	323	2.180	11	0.001092	2.42	22.07	0.53
LOHN4@10	33	35690	1072	349	2.675	10	0.001057	2.43	21.35	0.52
LOHN4@11	34	29955	888	350	2.651	10	0.000976	2.42	19.71	0.48
LOHN4@12	27	29155	1065	373	2.537	9	0.001080	2.46	21.82	0.54
LOHN4@13	26	23964	935	96	2.757	39	0.001066	2.13	21.54	0.46
LOHN4@14	28	22365	792	164	3.148	22	0.001104	2.33	22.31	0.52
LOHN4@15	24	20864	866	520	4.658	6	0.001039	2.55	20.99	0.53
LOHN4@16	30	23937	797	576	4.396	6	0.001002	2.62	20.25	0.53
LOHN4@19	27	21599	807	299	2.738	12	0.001075	2.41	21.71	0.52
LOHN4@20	29	23422	801	350	2.844	10	0.001042	2.43	21.05	0.51
LOHN4@21	16	17205	1046	169	2.252	22	0.001058	2.17	21.37	0.46
LOHN4@22	17	16983	991	164	2.244	23	0.001052	2.20	21.26	0.47
LOHN4@23	16	17269	1091	162	3.312	23	0.001073	2.29	21.67	0.50
LOHN4@24	20	21768	1108	175	2.589	21	0.000989	2.33	19.99	0.47
LOHN4@25	18	15361	875	177	2.812	21	0.000975	2.21	19.69	0.43
LOHN4@26	15	17857	1172	175	2.277	21	0.001004	2.17	20.29	0.44
LOHN4@27	27	26405	974	185	2.145	20	0.001055	2.23	21.32	0.47
LOHN4@28	28	27181	955	192	1.907	19	0.001071	2.29	21.63	0.50
LOHN4@29	27	25484	955	188	2.062	20	0.001046	2.33	21.13	0.49
LOHN4@30	27	25099	915	188	2.000	20	0.001064	2.22	21.49	0.48
LOHN4@31	30	25226	855	434	4.053	8	0.001139	2.49	23.00	0.57
LOHN4@32	36	21812	606	287	3.984	13	0.001060	2.42	21.42	0.52
LOHN4@33	27	23182	856	199	2.107	19	0.001001	2.21	20.23	0.45

https://doi.org/10.5194/se-2019-162
Preprint. Discussion started: 30 October 2019

	LOHN4@34	26	24807	948	185	2.031	20	0.001038	2.22	20.97	0.46
	LOHN4@35	25	23076	925	173	2.762	21	0.001042	2.49	21.06	0.52
	LOHN4@36	26	25326	972	187	2.009	20	0.001046	2.22	21.13	0.47
	LOHN4@37	27	26268	980	210	2.006	17	0.001061	2.33	21.44	0.50
	LOHN4@38	27	27571	1016	218	2.061	17	0.001033	2.30	20.86	0.48
	LOHN4@39	26	25481	988	209	2.005	18	0.001049	2.25	21.19	0.48
	LOHN4@40	26	26144	1007	211	2.322	17	0.001028	2.34	20.78	0.49
	LOHN4@41	19	24124	1248	224	2.175	16	0.001064	2.31	21.50	0.50
	LOHN4@42	19	23602	1235	227	2.195	16	0.001078	2.34	21.78	0.51
	LOHN4@43	21	23764	1157	237	2.977	15	0.001057	2.34	21.35	0.50
	LOHN4@44	20	23194	1138	231	2.863	16	0.001055	2.34	21.31	0.50
	LOHN4@45	20	23831	1188	232	2.181	16	0.001058	2.30	21.37	0.49
	LOHN4@46	20	20913	1027	204	2.406	18	0.001046	2.23	21.13	0.47
	LOHN4@48	22	23727	1093	262	2.358	14	0.001045	2.43	21.11	0.51
	LOHN4@49	22	23546	1065	259	2.356	14	0.001017	2.38	20.55	0.49
	LOHN4@50	21	22193	1049	267	2.394	13	0.001049	2.37	21.20	0.50
	LOHN4@51	20	22103	1121	259	2.442	14	0.001012	2.32	20.44	0.47
	LOHN4@52	20	20091	1023	242	3.200	15	0.000974	2.34	19.68	0.46
	LOHN4@53	10	15092	1539	136	2.130	28	0.001029	2.04	20.78	0.42
	LOHN4@54	10	13028	1330	135	2.234	28	0.000973	2.03	19.65	0.40
	LOHN4@55	10	14821	1515	139	2.261	27	0.000987	2.05	19.94	0.41
	LOHN4@05	19	14990	787	179	3.553	21	0.000893	2.55	18.03	0.46
	LOHN4@06	31	9191	298	150	5.119	26	0.000919	3.12	18.57	0.58
	LOHN4@17	32	23011	717	713	6.460	5	0.000936	3.16	18.91	0.60
B	**LOHN4@18**	39	23334	591	459	4.810	8	0.000924	2.85	18.68	0.53
	LOHN4@47	23	19054	816	222	2.582	17	0.000932	2.26	18.82	0.43
	LOHN4@56	9	11815	1254	128	2.946	30	0.000893	2.14	18.05	0.39
	LOHN4@57	13	11550	862	133	3.790	29	0.000846	2.67	17.09	0.46
	EUKL2@01	9	296	32	160	2.563	23	0.001042	1.75	21.06	0.37
	EUKL2@02	14	301	22	214	2.614	17	0.001095	2.15	22.11	0.47
	EUKL2@03	13	21097	1580	209	2.385	18	0.001075	1.91	21.71	0.41
	EUKL2@04	14	18352	1313	230	3.122	16	0.001058	1.83	21.36	0.39
	EUKL2@05	33	52673	1620	348	2.632	10	0.001077	1.98	21.77	0.43
	EUKL2@06	19	25562	1351	223	2.454	16	0.001100	1.81	22.23	0.40
	EUKL2@07	19	16767	868	234	2.768	15	0.001083	1.84	21.88	0.40

759

760

https://doi.org/10.5194/se-2019-162
Preprint. Discussion started: 30 October 2019

761 ***Table 5**: Summary of weighted mean ages of monazite growth domains and spot age ranges of each grain*

762 *from the TW.*

763

Sample domain	ID Nº	Figure	Table	Zoning of the grains	Weighted mean domain ages (Ma)	MSWD	Number of analyses	Spot age range of entire grain (Ma)	Reference
Western Tauern Window									
INNB1	**1**	3a	3	Regular	11.8 ± 0.5	2.8	7	12.6 ± 0.3 - 11.2 ± 0.7	this study
ZEI1 - A	**2**	3b	3	Regular	10.3 ± 0.3	1.9	14	11.0 ± 0.5 - 6.9 ± 0.4	this study
ZEI1 - B					10.0 ± 0.5	2.7	7		
ZEI1 - C					7.7 ± 0.9	2.4	4		
SCHR1 - A	**3**	3c	4	Regular	20.8 ± 0.6	1.7	6	21.8 ± 0.5 - 19.3 ± 0.5	this study
SCHR1 - B					20.3 ± 0.2	1.11	16		
SCHR1 - C					19.7 ± 0.4	0.97	6		
MAYR4	**4**	3d	3	Regular	–	–	–	12.8 ± 0.6 - 9.6 ± 0.5	this study
PFIT1 - A	**5**	3e	4	Patchy core	17.1 ± 0.4	1.4	9	17.8 ± 0.4 - 12.8 ± 0.4	this study
PFIT1 - B					13.1 ± 0.3	0.76	5		
BURG2	**6**	3f	3	Regular	–	–	–	18.4 ± 0.9 - 13.9 ± 0.9	this study
PLAN1 - A	**7**	3g	3	Patchy core	13.0 ± 0.2	0.86	17	13.7 ± 0.7 - 8.4 ± 0.6	this study
Central Tauern Window									
SCHEI1 - A	**8**	4a	3	Regular	18.0 ± 0.2	2.2	20	19.0 ± 0.4 - 16.0 ± 0.4	this study
SCHEI1 - B					16.5 ± 0.4	0.74	4		
HOPF2 - B and C	**9**	4b	4	Regular	12.1 ± 0.3	2.9	14	13.5 ± 0.3 - 10.9 ± 0.3	this study
GART1 - A	**10**	4c	3.00	Regular	17.0 ± 0.2	1.2	10	17.8 ± 0.4 - 16.3 ± 0.5	this study
GART1 - B					16.9 ± 0.3	1.3	9		
NOWA3 - A	**11**	4d	3	Regular	17.1 ± 0.7	2.6	6	18.3 ± 0.5 - 16.0 ± 0.8	this study
NOWA3 - B					17.3 ± 0.4	0.82	5		
NOWA3 - C					17.2 ± 0.9	1.6	5		
GART3 - A	**12**	4e	3	Regular	18.3 ± 1.2	1.6	6	20.2 ± 0.9 - 15.2 ± 0.9	this study
GART3 - B					17.3 ± 0.8	2.3	9		
GART3 - C					16.0 ± 0.8	0.41	5		
STEI2	**13**	4f	3	Regular / Patchy tail	17.6 ± 0.2	1.4	20	18.6 ± 0.3 - 17.1 ± 0.4	this study
KNOR1 - A	**14**	4g	4	Regular	10.7 ± 0.5	1.7	5	11.6 ± 0.4 - 10.0 ± 0.2	this study
KNOR1 - B					10.5 ± 0.2	1.5	8		
KNOR1 - C					10.3 ± 0.2	1.4	8		

https://doi.org/10.5194/se-2019-162
Preprint. Discussion started: 30 October 2019

Eastern Tauern Window

KAIS6 - A	**15**	5a	4	Patchy border	21.1 ± 0.4	0.71	6	21.8 ± 0.5 - 16.9 ± 0.5	this study
KAIS6 - B					20.8 ± 0.2	0.58	24		
KAIS6 - C					20.6 ± 0.3	0.56	7		
SALZ18-A	**16a**	5b	4	Regular	18.2 ± 0.4	2.8	14	19.3 ± 0.5 - 15.7 ± 0.4	this study
T3	***16b***		-	*Regular*	*18.1 ± 0.4*	*0.51*	*4*	*18.5 ± 0.4 - 14.8 ± 0.4*	*Gnos et al., 2015*
					17.2 ± 0.5	*3.4*	*10*		
					16.0 ± 0.3	*0.51*	*8*		
					15.5 ± 0.2	*0.74*	*24*		
LOHN4 - A	**17**	5c	4	Patchy core	21.0 ± 0.2	2.3	50	23.0 ± 0.6 - 17.1 ± 0.5	this study
LOHN4 - B					18.2 ± 0.6	1.8	7		
ORT1	**18**	5d	3	Regular	20.1 ± 0.3	0.82	13	21.1 ± 0.7 - 19.6 ± 0.8	this study
EUKL2	**19a**	5e	4	Regular	21.7 ± 0.3	1.08	7	22.2 ± 0.4 - 21.1 ± 0.4	this study
T2	***19b***		-	*Patchy*	*15.1 ± 0.5*	*0.26*	*4*	*15.4 ± 0.4 - 15.0 ± 0.7*	*Gnos et al., 2015*
HOAR1-A	**20**	5f	3	Patchy	22.3 ± 0.6	3.0	24	24.9 ± 1.9 - 19.4 ± 1.3	this study
HOAR1-B					20.7 ± 1.2	2.9	5		
T1	***21***		-	*Regular*	*19.0 ± 0.5*	*0.51*	5	*19.2 ± 0.5 - 14.3 ± 0.5*	*Gnos et al., 2015*
					17.6 ± 0.6	*1.6*	8		
					16.3 ± 0.6	*3.0*	12		
					15.0 ± 0.5	*1.7*	8		
T4	***22***		-	*Patchy*	*15.6 ± 0.7*	*9.1*	*21*	*18.3 ± 1.1 - 13.1 ± 0.8*	*Gnos et al., 2015*
MOKR1 - A	**23**	5g	3	Regular	20.6 ± 0.7	1.4	15	22.8 ± 1.1 - 14.3 ± 0.9	this study
MOKR1 - B					20.6 ± 0.6	2.0	12		
SAND1 - A	**24**	5h	3	Regular	21.3 ± 2.1	2.0	5	24.8 ± 1.2 - 17.2 ± 1.1	this study
REIS1	**25**	5i	3	Regular	17.3 ± 1.2	2.6	13	21.3 ± 1.0 - 10.14 ± 1.38	this study

764